nature biomedical engineering

SUPPLEMENTARY INFORMATION

https://doi.org/10.1038/s41551-020-0547-4

In the format provided by the authors and unedited.

Ultrabright fluorescent nanoscale labels for the femtomolar detection of analytes with standard bioassays

Jingyi Luan[1], Anushree Seth[1], Rohit Gupta[1], Zheyu Wang[1], Priya Rathi[1], Sisi Cao[1], Hamed Gholami Derami[1], Rui Tang[2], Baogang Xu[2], Samuel Achilefu[2], Jeremiah J. Morrissey[3,4] and Srikanth Singamaneni[1,4] ✉

[1]Department of Mechanical Engineering and Materials Science, Institute of Materials Science and Engineering, Washington University in St. Louis, St Louis, MO, USA. [2]Department of Radiology, Washington University School of Medicine, St. Louis, MO, USA. [3]Department of Anesthesiology, Division of Clinical and Translational Research, Washington University in St. Louis, St. Louis, MO, USA. [4]Siteman Cancer Center, Washington University in St. Louis, St. Louis, MO, USA. ✉e-mail: singamaneni@wustl.edu

Table of contents

Calculation of the protein/biotin ratio: BSA/biotin ratio was calculated through 4-Hydroxyazobenzene-2-carboxylic acid (HABA) assay. Specifically, biotinylated BSA (0.4 mg/ml×100 µl) was added to a mixture of HABA (Thermo Scientific, 1854180) and avidin solution (900 µl, Thermo Scientific, 21121). Due to its higher affinity to avidin, biotin replaced HABA from avidin and the absorbance at 500 nm decreased proportionally (Figure S4). The change in the absorbance was calculated using the following equation:

$$\Delta A_{500} = (0.9 \times A_{500}) - A_{500}B$$

where A_{500} and $A_{500}B$ represent the absorbance of HABA/avidin before and after the addition of biotinylated BSA, respectively. A correction factor (0.9) was employed to adjust for the dilution of HABA/avidin solution by adding biotinylated BSA. The concentration of the sample can be calculated using Beer's Law:

$$A_\lambda = \varepsilon_\lambda bC$$

where A_λ is the absorbance of the sample at wavelength λ nm (ΔA_{500}), ε_λ represents the extinction coefficient at wavelength λ nm (34,000 $M^{-1}cm^{-1}$), b is the cell path length (1 cm using quartz cuvette), and C is the concentration of the sample. Using this equation, biotin concentration was calculated to be:

$$\mathrm{C}\left(\frac{\mathrm{mmol}}{\mathrm{ml}}\right) = \frac{\Delta A_{500}}{34{,}000 \times b} = \frac{0.1765}{34{,}000} = 5.19 \times 10^{-6}\ \mathrm{mmol/ml}$$

BSA concentration was 6×10^{-7} mmol/ml. On an average, 8.7 biotin molecules were conjugated to BSA molecule. Similarly, dye to protein ratio was calculated using the following equation:

$$\left(\frac{A_{780}}{\varepsilon_{Dye}}\right) / \left(\frac{A_{280} - 0.03 \times A_{780}}{\varepsilon_{protein}}\right)$$

where 0.03 is the correction factor for the absorbance of 800CW at 280 nm, $\varepsilon_{Dye}(270{,}000\ M^{-1}cm^{-1})$ and $\varepsilon_{protein}$ $(43{,}824\ M^{-1}cm^{-1})$ are the extinction coefficients for 800CW and BSA respectively, and $A_{780} = 0.3$ and $A_{280} = 0.05$ are the absorbance of BSA-800CW at 780 nm and 280 nm, respectively (Figure S5). The final dye to protein ratio was therefore calculated to be 1.2.

Fluorescence lifetime measurements: Fluorescence lifetimes (FLT) were measured using Time-Correlated Single Photon Counting (TCSPC, implemented in Fluorolog-3, Horiba Jobin Yvon) with a 740 nm excitation source NanoLed® (impulse repetition rate 1 MHz) at 90º to the PMT R928P detector (Hamamatsu Photonics, Japan). The detector was set to 800 nm with a 20 nm bandpass and data were collected until the peak signal reached 2,000 counts. The details of the system have been published in previous studies[1,2]. The instrument response function was obtained using a Rayleigh scatter of Ludox-40 (0.05% in MQ water; Sigma-Aldrich) in an acrylic transparent cuvette at 740 nm emission. Lifetime values were obtained by fitting the decay curve using Decay analysis software (DAS6 v6.8; Horiba), based on

$$\mathrm{I(t)} = \sum_{i=1}^{n} \mathrm{I}(0) * \exp\left(\frac{-t}{\tau}\right)$$

where I represents the fluorescence intensity, t represents decay time and τ represents lifetime. The quality of fit was judged by χ^2 values, Durbin–Watson parameters, as well as visual observations of fitted line, residuals, and autocorrelation functions. The fitting (biexponential fitting) provided two values of the fluorescence lifetime: τ_1 and τ_2 as listed in the table below (Table S1). Since τ_2 is extremely large compared to that of common fluorophore and showed insignificant contribution (<5%), we regard this value as background noise. The reason to use biexponential fitting is to fit the environment photons out (usually have longer lifetime) to get a cleaner 1st exponential value for the real fluorescence lifetime.

Samples	τ_1	τ_2 (background)	χ^2
CW800-BSA	0.722 ns (95.42%)	4.81 ns (4.58%)	1.014
Plasmonic-fluor-800CW	0.178 ns (93.12%)	4.77 ns (4.41%)	1.107

Table S1. Fluorescence lifetimes and χ^2 obtained using biexponential fit.

Calculation of quantum yield: The radiative and nonradiative decay rate can be calculated from the measured lifetime and quantum yield of 800CW (conjugated to BSA)[3]:

$$\Gamma = \frac{Q_0}{\tau_0} = 0.15\ ns^{-1}$$

$$k_{nr} = \frac{1}{\tau_0} - \Gamma = 1.2\ ns^{-1}$$

where Γ and k_{nr} represent radiative and non-radiative decay rate of 800CW. Q_0 (11%) and τ_0 $(0.74\ ns)$ represent the measured quantum yield (Figure S7) and lifetime of 800CW. Here, we assumed that k_{nr} remains unaltered after conjugating the fluorophore to AuNR (due to minimal quenching observed). Therefore, the radiative rate enhancement of 800CW (Γ_{AuNR}) and improved quantum yield induced by AuNR (Q_{AuNR}) can be calculated as[3]:

$$\Gamma_{AuNR} = \frac{1}{\tau_{AuNR}} - k_{nr} = 4.4\ ns^{-1}$$

$$Q_{AuNR} = \Gamma_{AuNR} * \tau_{AuNR} = 0.79$$

where τ_{AuNR} $(0.179\ ns)$ represents the average lifetime of 800CW after its conjugation to AuNR. The result shows that the fluorophore quantum yield is improved by 7-fold (from 11% to 79%) upon conjugation to AuNR with optimal optical properties and spacer layer.

Estimation of the amount of 800CW absorbed on plasmonic-fluor-800CW: To estimate the amount of fluorophore on AuNR, we first estimated the amount of BSA (-conjugate) using the bicinchoninic acid assay (BCA assay). From the amount of BSA, 800CW concentration can be calculated as the dye to protein ratio has been determined to be 1.2 (described above). Micro BCA protein assay kit (Thermo Scientific, product number 23235, lot number QG218473A) was employed for the test. Specifically, BCA working reagent was prepared by mixing 2.5 ml of reagent MA, 2.4 ml of reagent MB, and 0.1 ml of reagent MC. 150 µl of BSA standards (from 0 to 40 µg/ml) or plasmonic-fluor-800CW (extinction~4.6) was mixed with 150 µl of the working reagent and the mixture was incubated in 60 °C for 1 hour. The absorbance at 562 nm was measured by a plate reader and a BSA standard curve was obtained. The concentration of BSA absorbed around plasmonic-fluor-800CW was calculated to be 6.2 µg/ml based on the standard curve. Therefore, plasmonic-fluor-800CW with extionction~0.63 is comprised of ~0.9 µg/ml of BSA (~13.5 nM) and ~16.2 nM of 800CW.

Based on the report by El-Sayed *et al* and other groups[4-6], the extinction coefficient of AuNR (length~83 nm and diameter~24 nm) was calculated to be $\varepsilon \approx 8.27\times10^9$ (L M^{-1} cm^{-1}). Molar concentration of the AuNR corresponding to optical extinction of 0.63 can be derived from Beer's

Law, which is calculated to be 76.2 pM. Therefore, the number of 800CW (n) on a single AuNR can be calculated based on:

$$n = \frac{C_{800CW}}{C_{AuNR}} = 210$$

Where C_{800CW} (16 nM) and C_{AuNR} (76.2 pM) represent the molar concentration of 800CW and AuNR, respectively.

Figure

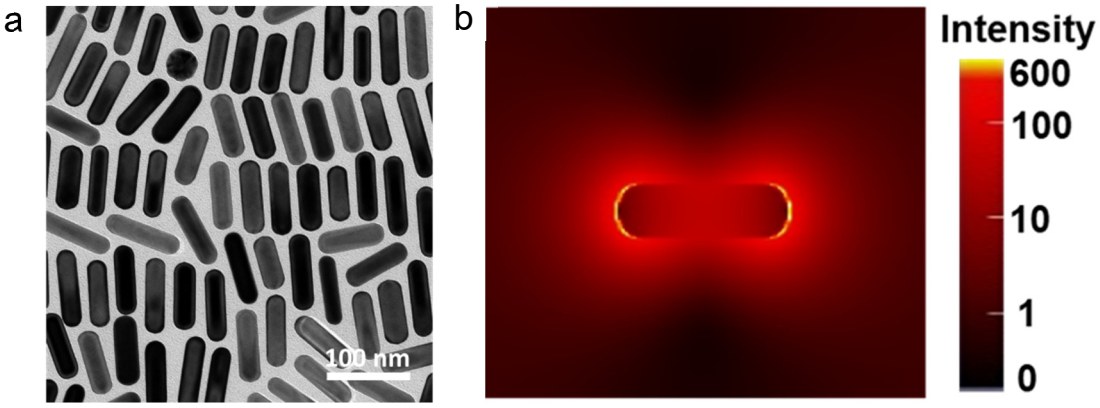

Figure S1. (a) TEM image of gold nanorod (AuNR) employed as the nanoantennae in plasmonic-fluor-800CW. (b) Finite-difference time-domain (FDTD) simulation showing the distribution of electric field intensity around the AuNR (polarization of the incident beam is along the long-axis of the AuNR).

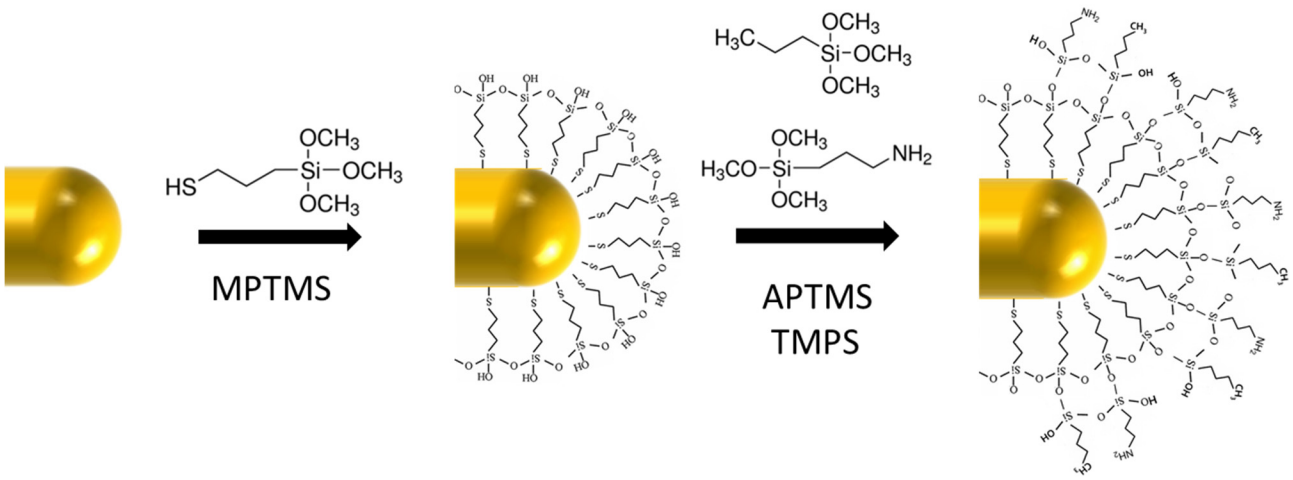

Figure S2. Schematic illustration showing the steps involved in the formation of polymer spacer on AuNR.

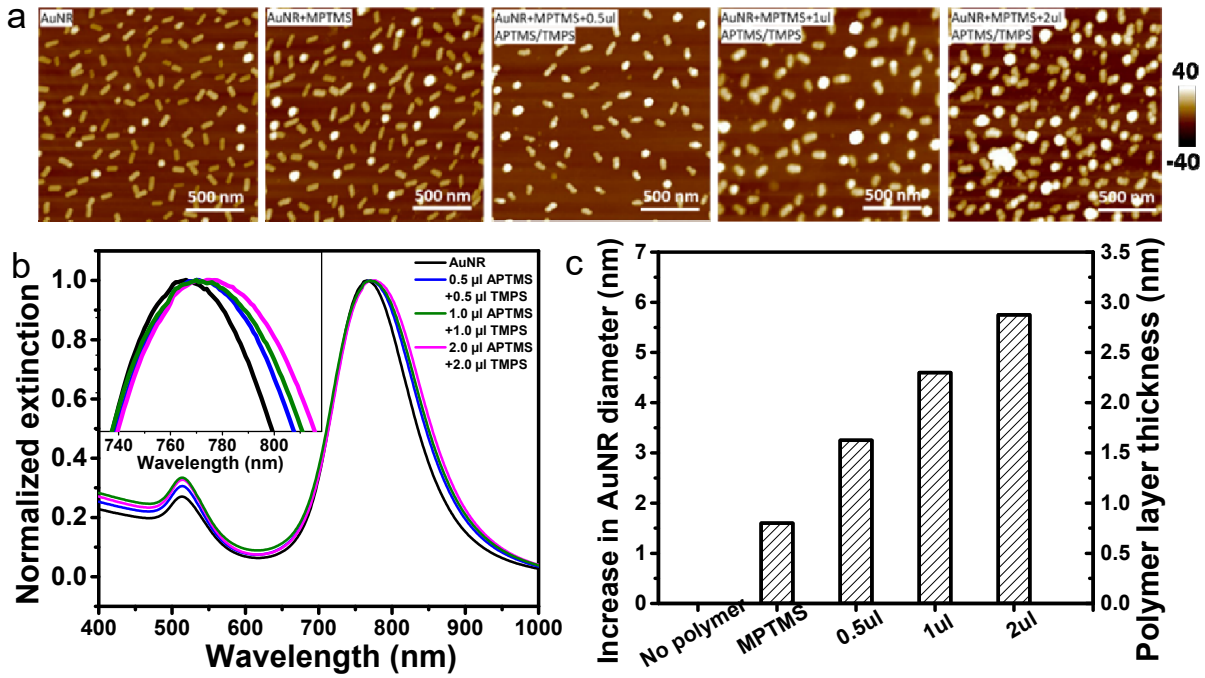

Figure S3. (a) AFM image depicting an increase in the diameter of AuNR/polymer under increasing amount of monomer (MPTMS, TMPS, and APTMS). (b) UV-vis spectra of AuNR under different polymerization conditions. (c) Plot showing an increase in the diameter of AuNR (two-fold higher than polymer layer thickness) under each polymerization condition measured from AFM images.

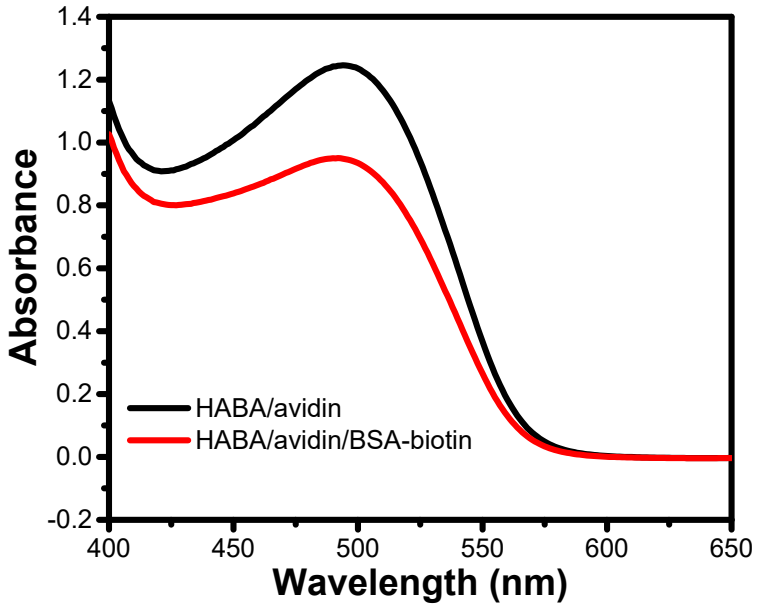

Figure S4. Absorbance spectra of HABA/avidin and HABA/avidin/BSA-biotin. Due to the stronger affinity to avidin, biotin replaces the HABA bound to avidin and causes a decrease in the absorbance intensity.

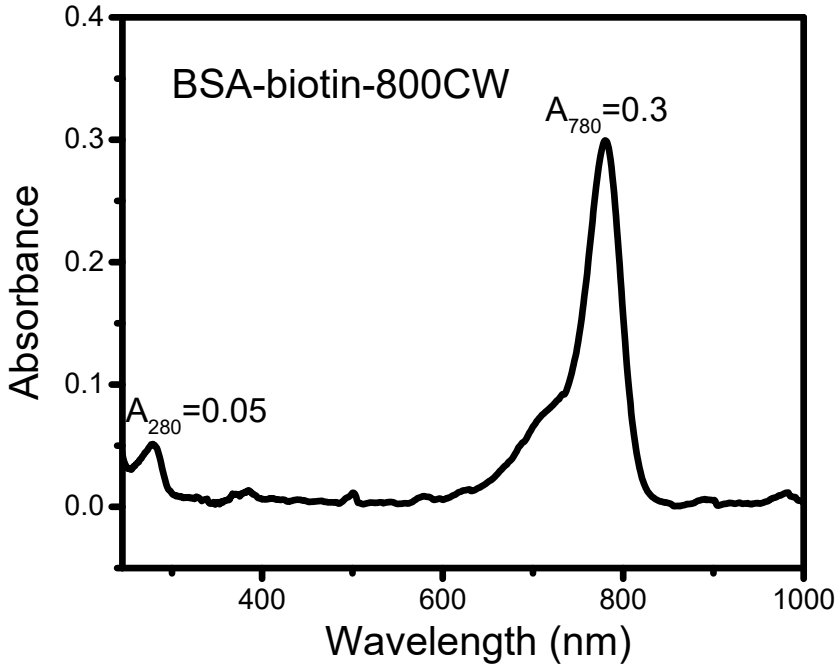

Figure S5. Absorbance spectrum of BSA-biotin-800CW conjugate measured using quartz cuvette with a cell path length of ~1 cm. The absorbance values at 780 nm and 280 nm were employed to quantify the dye to BSA ratio.

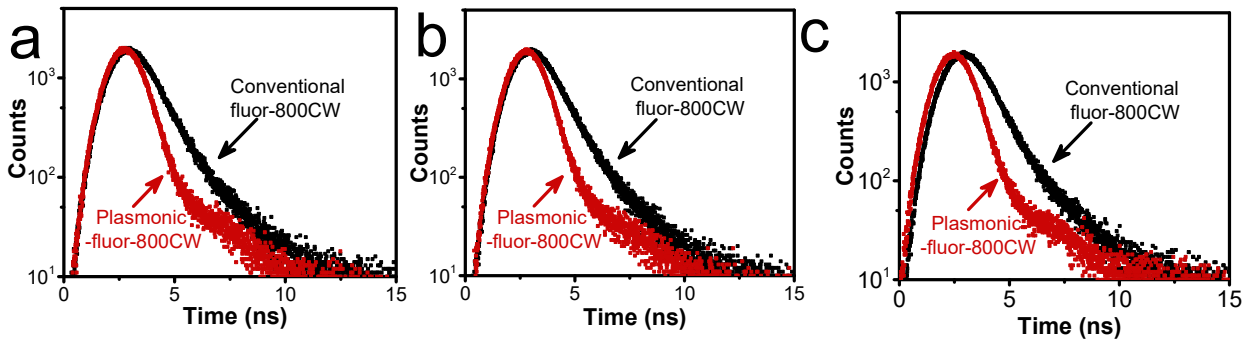

Figure S6. Independent measurements (performed with different batches of plasmonic-fluors synthesized on different days) of fluorescence lifetime of conventional fluor (free CW800 conjugated on BSA) and plasmonic-fluor-800CW.

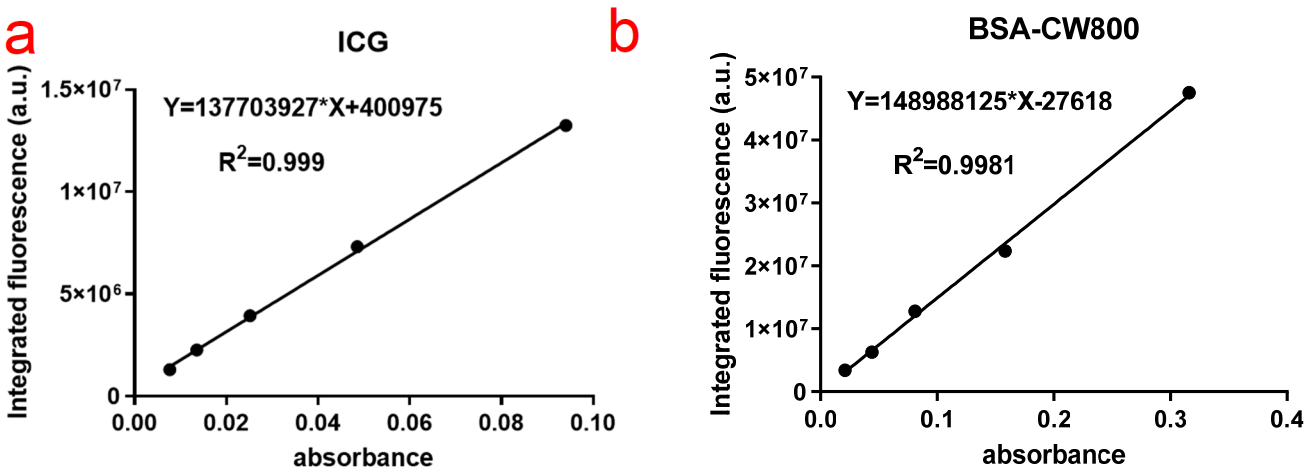

Figure S7. Integrated fluorescence of ICG and BSA-CW800 under different absorbance. The quantum yield of 800CW (conjugated to BSA) was determined to be ~11%.

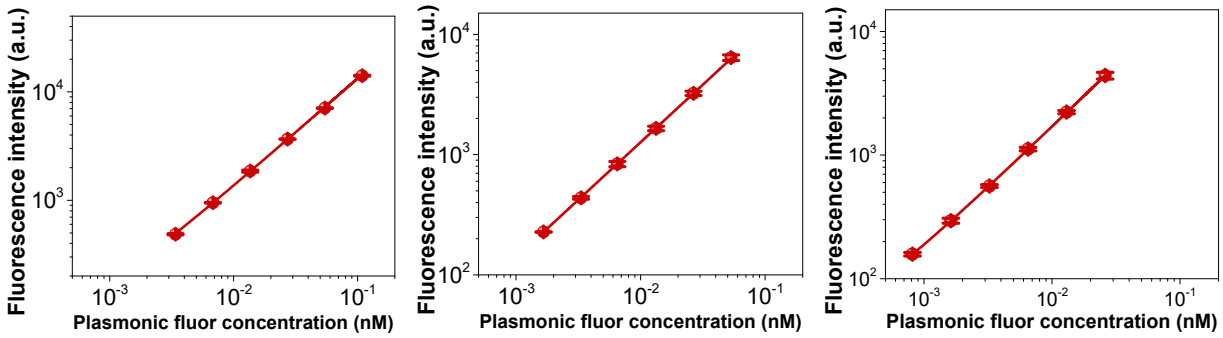

Figure S8. Fluorescence intensity of different batches of plasmonic-fluor-800CW at different molar concentrations. The slopes of the curves indicate that the plasmonic-fluor-800CW exhibits 6700 (± 900)-fold higher brightness than the corresponding fluorophore. Error bar, s.d. (n=3 repeated tests).

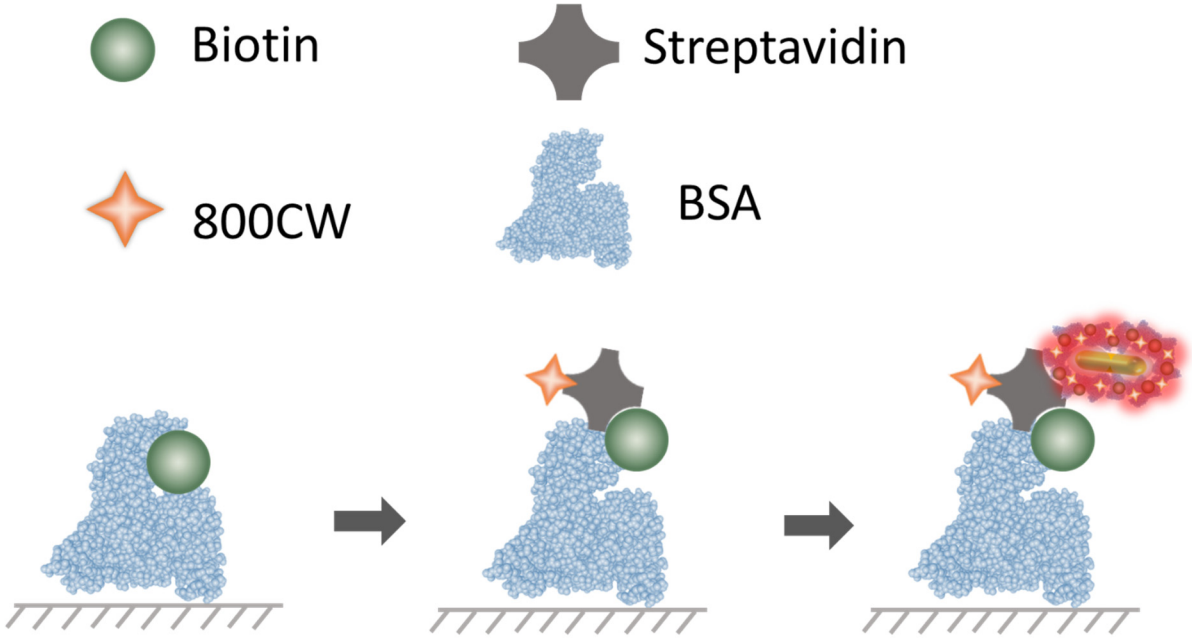

Figure S9. Schematic illustration (not to scale) showing the model system based on the binding events that occur in fluorophore-labeled immunosorbent assay.

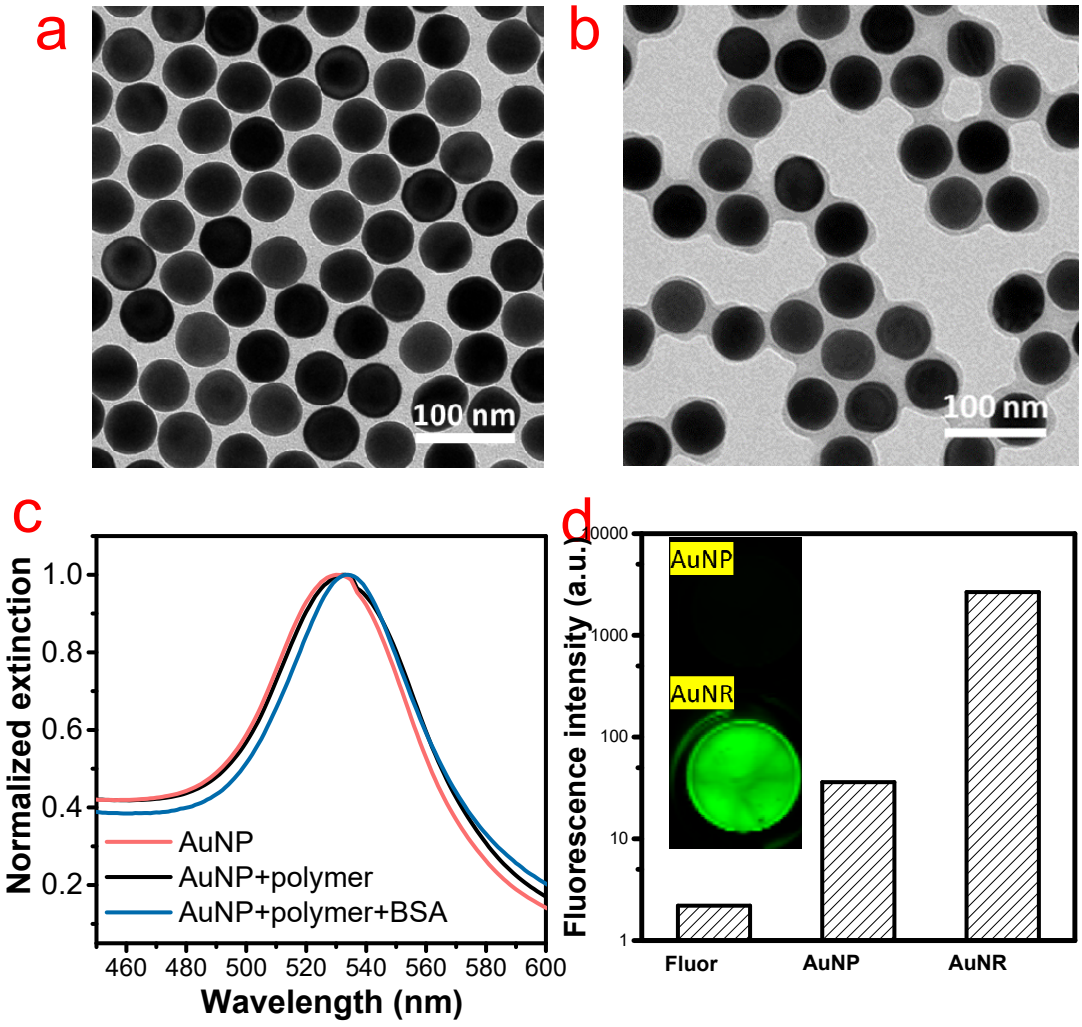

Figure S10. (a) TEM image of gold nanoparticle (AuNP) with a diameter of ~50 nm. (b) TEM image of AuNP after being coated with polymer spacer and BSA-800CW-biotin (AuNP-plasmonic-fluor-800CW). (c) UV-vis spectra of AuNP, AuNP coated with polymer spacer, and AuNP coated with polymer and BSA (BSA-biotin-800CW), showing a continuous red shift after each coating step. (d) Fluorescence intensity obtained using AuNP- and AuNR-plasmonic-fluor (compared with conventional fluorophore).

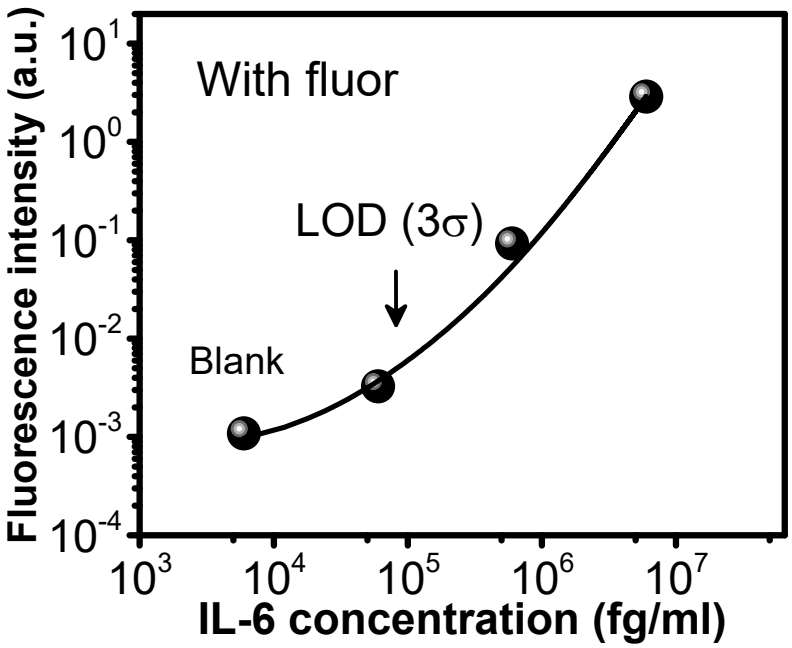

Figure S11. LOD of conventional IL-6 FLISA. The standard curve was generated using polynomial fitting. Each data point represents the average value of duplicate tests, which are included in supporting information.

Human IL-6 FLISA				
	Data 1	Data 2	Mean	S.D.
6ng/ml	2.930	2.843	2.887	0.062
600pg/ml	0.123	0.060	0.092	0.045
60pg/ml	0.002	0.004	0.003	0.002
6pg/ml	0.000	0.149	0.075	0.106
600fg/ml	0.007	0.002	0.004	0.003
60fg/ml	0.009	0.002	0.005	0.005
6fg/ml	0.000	0.000	0.000	0.000
0	0.002	0.000	0.001	0.002

Human IL-6 p-FLISA				
	Data 1	Data 2	Mean	S.D.
6ng/ml	4060	4240	4150	127.28
600pg/ml	2590	2780	2685	134.35
60pg/ml	746	714	730	22.63
6pg/ml	130	125	127.5	3.54
600fg/ml	37.8	38.1	37.95	0.21
60fg/ml	29.5	27.2	28.35	1.63
6fg/ml	18.6	18.9	18.75	0.21
0	16.3	16.8	16.55	0.35

Human IL-6 ELISA				
	Data 1	Data 2	Mean	S.D.
6ng/ml	3.382	3.318	3.350	0.046
600pg/ml	2.508	2.458	2.483	0.035
60pg/ml	0.560	0.576	0.568	0.011
6pg/ml	0.105	0.101	0.103	0.002
600fg/ml	0.048	0.048	0.048	0.000
60fg/ml	0.042	0.043	0.042	0.001
6fg/ml	0.042	0.047	0.044	0.003
0	0.051	0.041	0.046	0.007

Figure S12. Individual data points, mean value, and standard deviation from human IL-6 FLISA, p-FLISA, and ELISA.

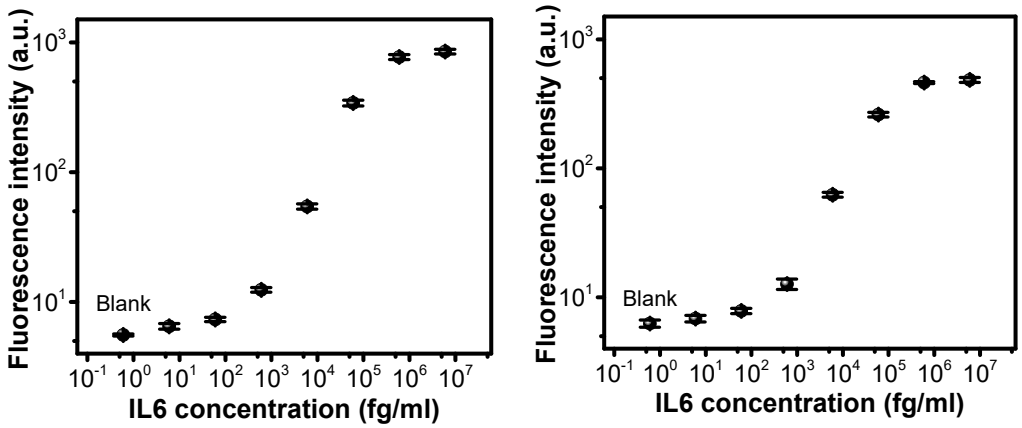

Figure S13. Plots showing the IL-6 dose-dependent fluorescence intensity from p-FLISA. The data represents experiments that were performed independently on different days with different batches of plasmonic-fluor-800CW. Error bar, s.d. (n=3 repeated tests).

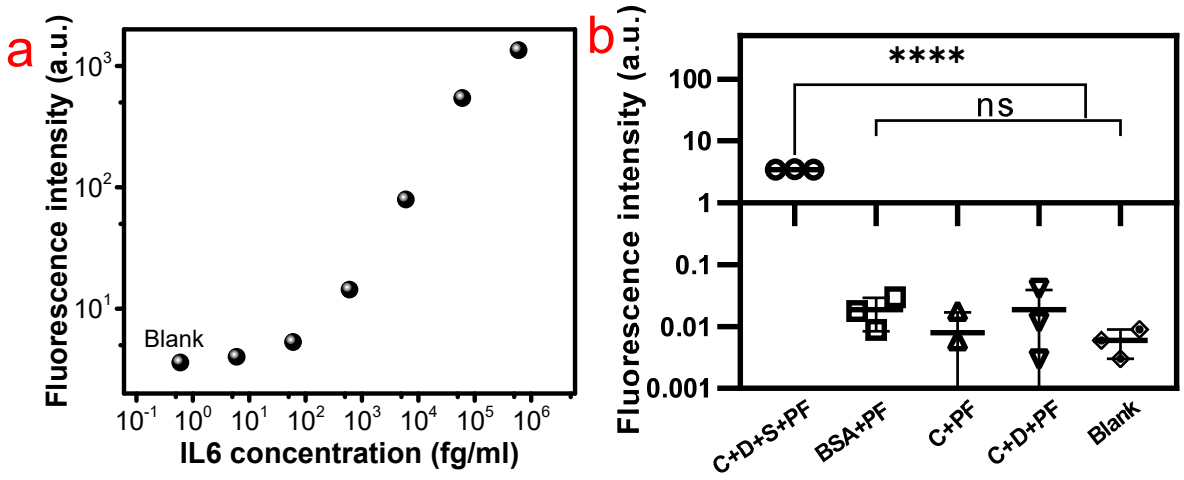

Figure S14. (a) IL-6 dose-dependent fluorescence intensity from p-FLISA. Each data point represents the average value of duplicate tests. (b) Non-specific binding of plasmonic-fluor-800CW. C: capture antibody; D: detection antibody; S: streptavidin; PF: plasmonic-fluor; Blank: no plasmonic-fluor. Compared to blank, no signal was observed after applying plasmonic-fluor-800CW to BSA, capture antibody, or capture and detection antibody. **** $P < 0.0001$ by one-way ANOVA with Tukey's post test. NS: not significant. Non-specific signal at zero concentration of IL-6 was present only when streptavidin was introduced, implying excellent specificity of plasmonic-fluor. Error bar, s.d. (n=3 repeated tests).

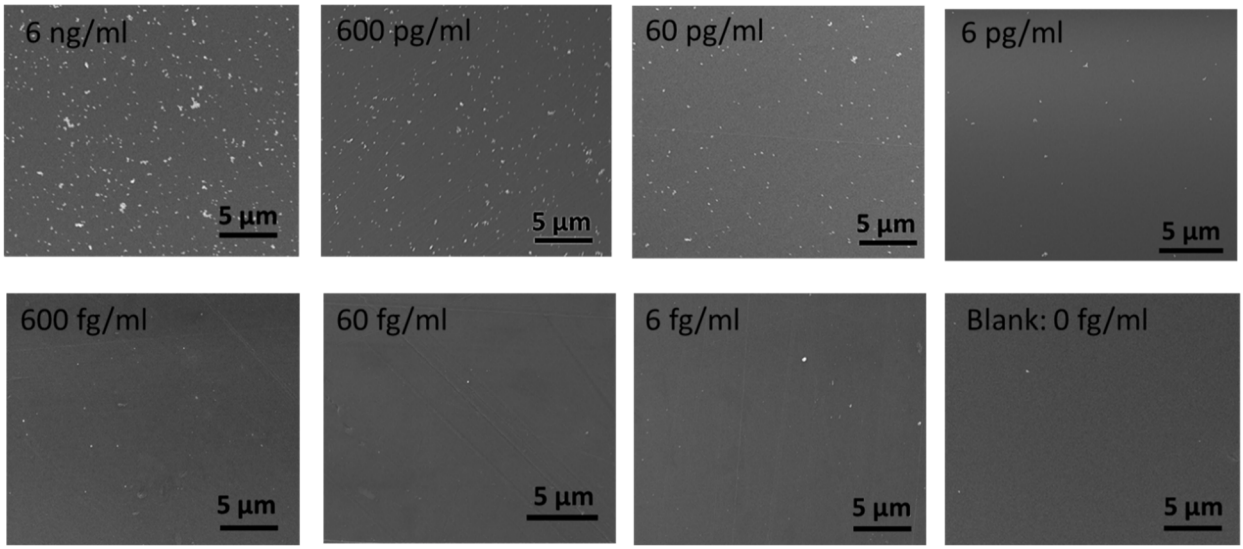

Figure S15. SEM images of the bottom surface of 96-well plate following IL-6 p-FLISA, revealing an increasing density of plasmonic-fluor-800CW with increasing concentration of IL-6.

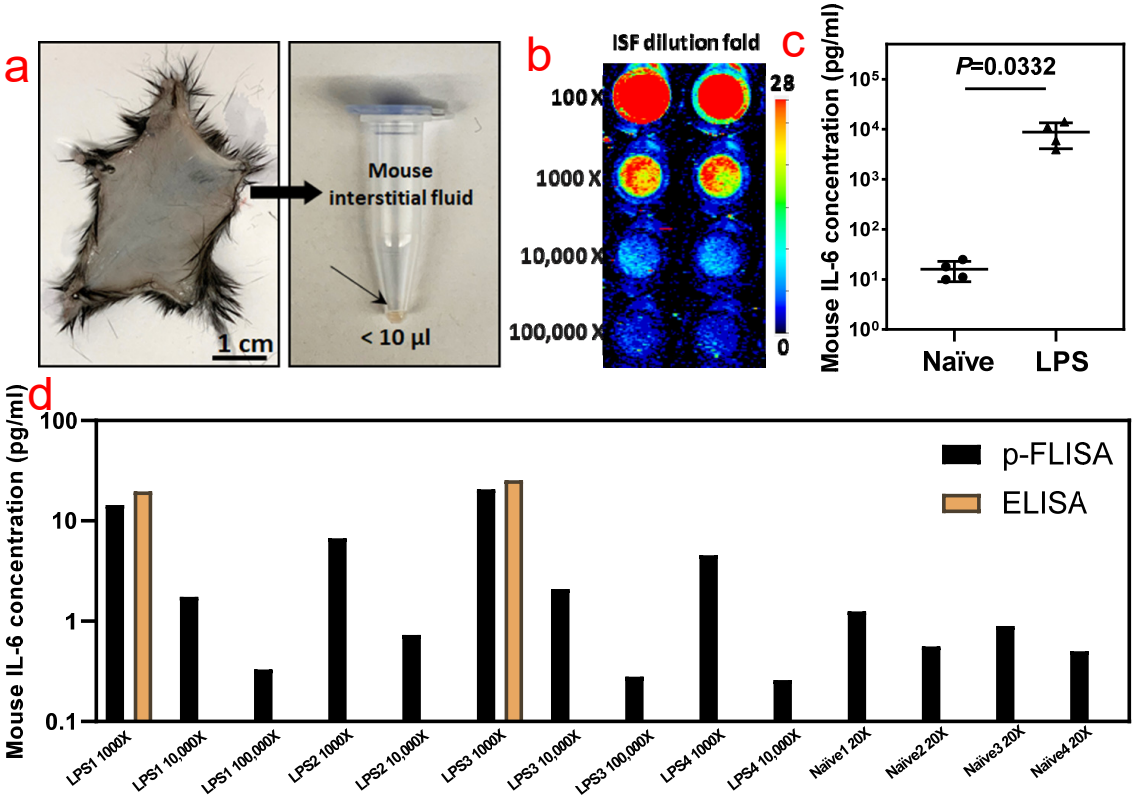

Figure S16. (a) Left: Photograph showing the whole mouse back skin used for collecting interstitial fluid (ISF). Right: Photograph showing the extremely small amount of ISF (~10 µL) collected from the entire mouse skin shown in the left image. (b) Fluorescence map corresponding to the ISF IL-6 concentrations in LPS injected mouse at different dilution factors of ISF, demonstrating the large dynamic range of p-FLISA. (c) IL-6 concentrations in ISF of naïve mice and immune-stimulated mice, measured using p-FLISA. Error bar, s.d. N = 4 biologically independent mice samples. Data statistically significant P value= 0.0332, * $P < 0.05$ by two-tailed unpaired t-test with Welch's correction. (d) Mouse IL-6 concentrations in ISF after serial dilutions measured by p-FLISA and ELISA. P-FLISA enabled the detection and quantification of IL-6 concentrations in ISF from naïve mice and LPS injected mice at all of the dilutions, most of which cannot be detected using conventional ELISA.

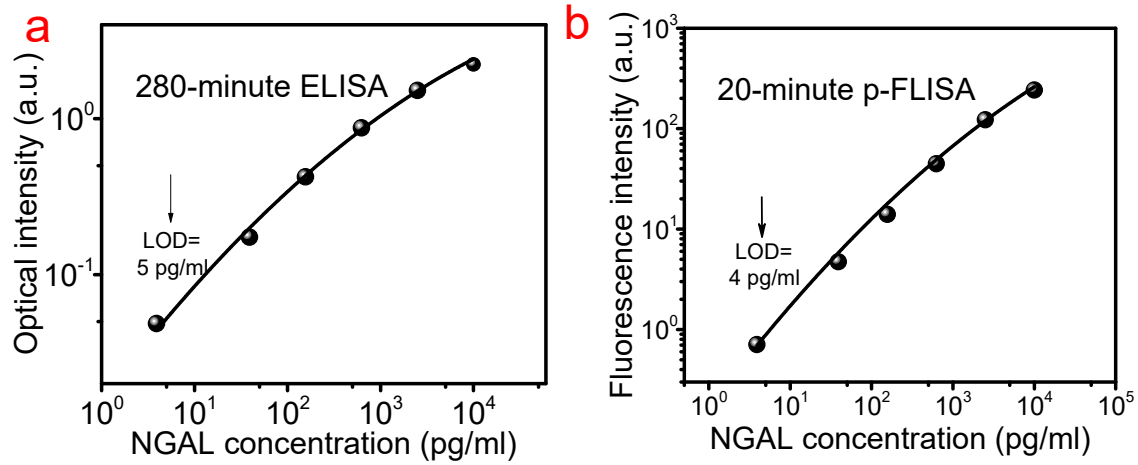

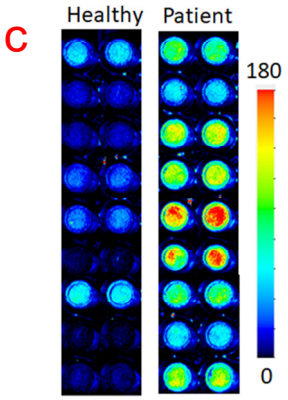

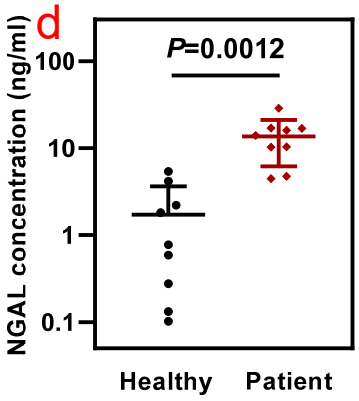

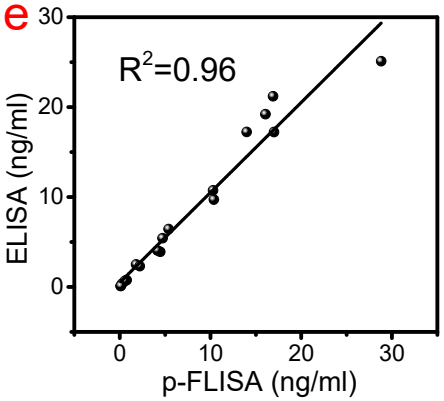

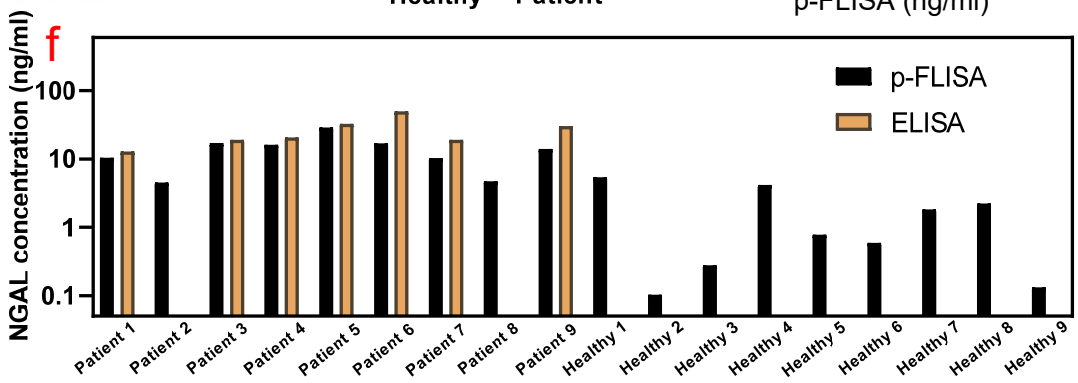

g

Patient number	age	gender		Healthy volunteer number	age	gender
1	89	male		1	28	female
2	67	male		2	29	male
3	31	female		3	29	male
4	61	male		4	26	male
5	49	female		5	25	male
6	68	female		6	25	male
7	73	female		7	28	female
8	59	male		8	28	female
9	63	male		9	26	male

Figure S17. (a) Plot showing the ELISA standard curve of human NGAL. The total reagent incubation time required for gold standard ELISA is 280 minutes with a limit of detection around 5 pg/ml. (b) Plot showing the p-FLISA standard curve of human NGAL. The total reagent incubation time of p-FLISA is significantly shortened to only 20 minutes while achieving similar sensitivity as the 280-minute ELISA. Each data point represents the average value of duplicate tests. (c) Fluorescence intensity maps of p-FLISA corresponding to urinary NGAL concentrations in samples of 9 self-described healthy individuals and 9 kidney disease patients. (d) Plot showing NGAL concentrations of self-described healthy individuals and kidney disease patients based on p-FLISA tests. The urine samples were diluted by 10-fold before the assay. Error bar, s.d. N = 10 biologically independent patients' (or healthy volunteers') samples. Data statistically significant P value= 0.0012, ** $P < 0.05$ by two-tailed unpaired t-test with Welch's correction. (e) Comparison of NGAL concentrations measured by gold standard ELISA (280 minutes) and p-FLISA (20 minutes), showing a good correlation (R^2=0.96). (f) Comparison of the NGAL concentrations measured by 20-minute p-FLISA and 20-minute ELISA. NAGL concentrations from some patients and all the healthy volunteers cannot be detected by 20-minute ELISA. (g) Demographic information of patients and healthy volunteers

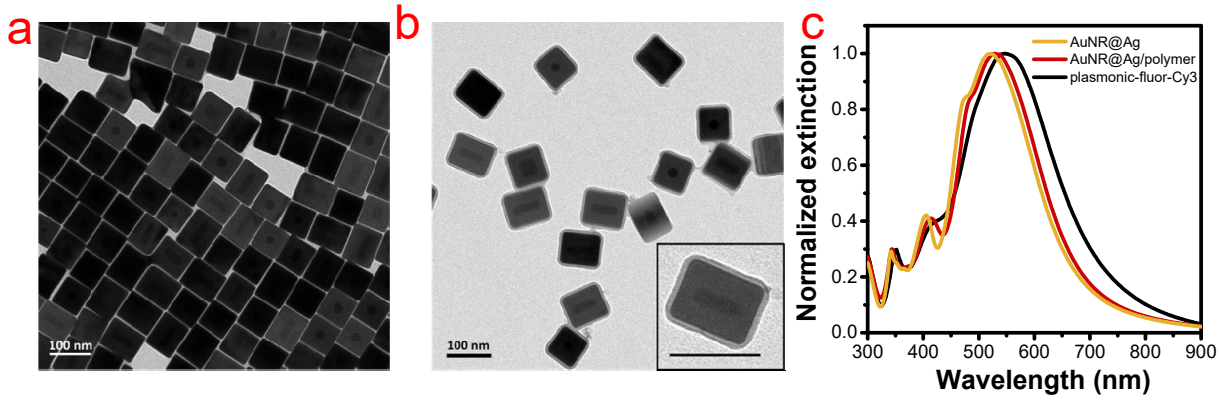

Figure S18. TEM image of (a) AuNR@Ag nanocuboids and (b) plasmonic-fluor-Cy3, which consists of AuNR@Ag nanocuboids, polymer shell, and a coating of BSA-biotin-Cy3. (c) UV-vis spectra of AuNR@Ag nanocuboids, AuNR@Ag nanocuboids coated with polymer spacer, and plasmonic-fluor-Cy3, revealing a continuous red shift after each coating step.

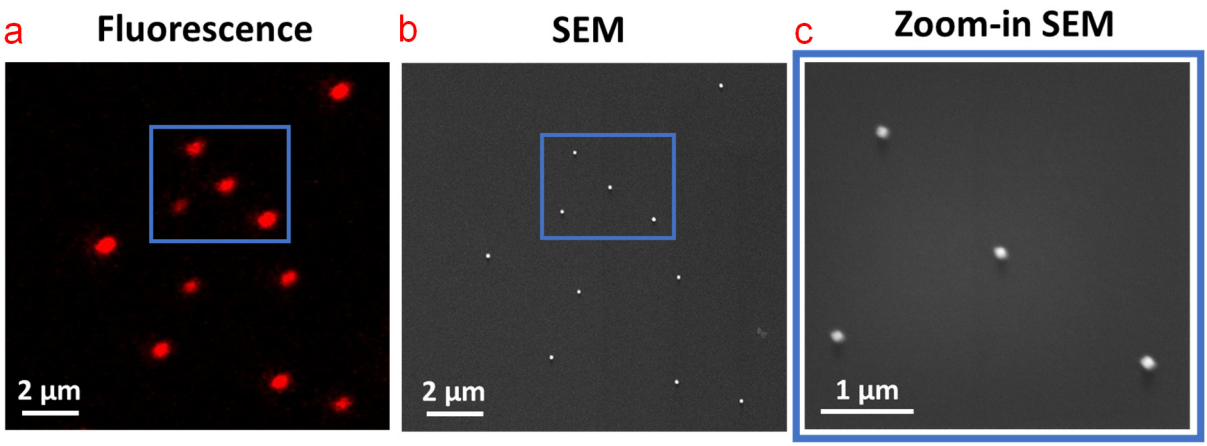

Figure S19. (a) Fluorescence microscopic image and (b) corresponding SEM images of individual plasmonic-fluor-Cy3. (c) Zoom-in SEM image showing single plasmonic-fluor-Cy3 (single nanocuboid). The fluorescence image was acquired by a non-laser epifluorescence microscope, which is widely available in common research labs.

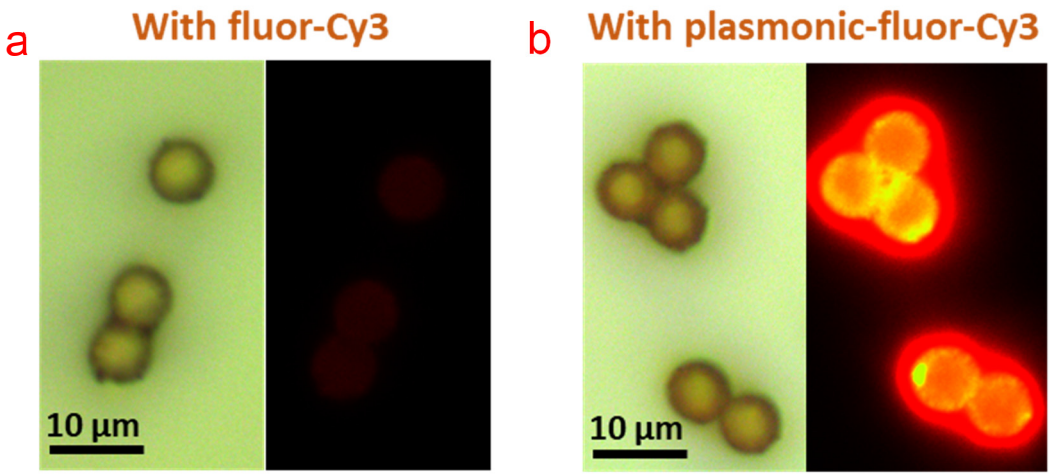

Figure S20. Microscopic bright field image and fluorescence image of Luminex microbeads (a) before and (b) after being probed by plasmonic-fluor-Cy3.

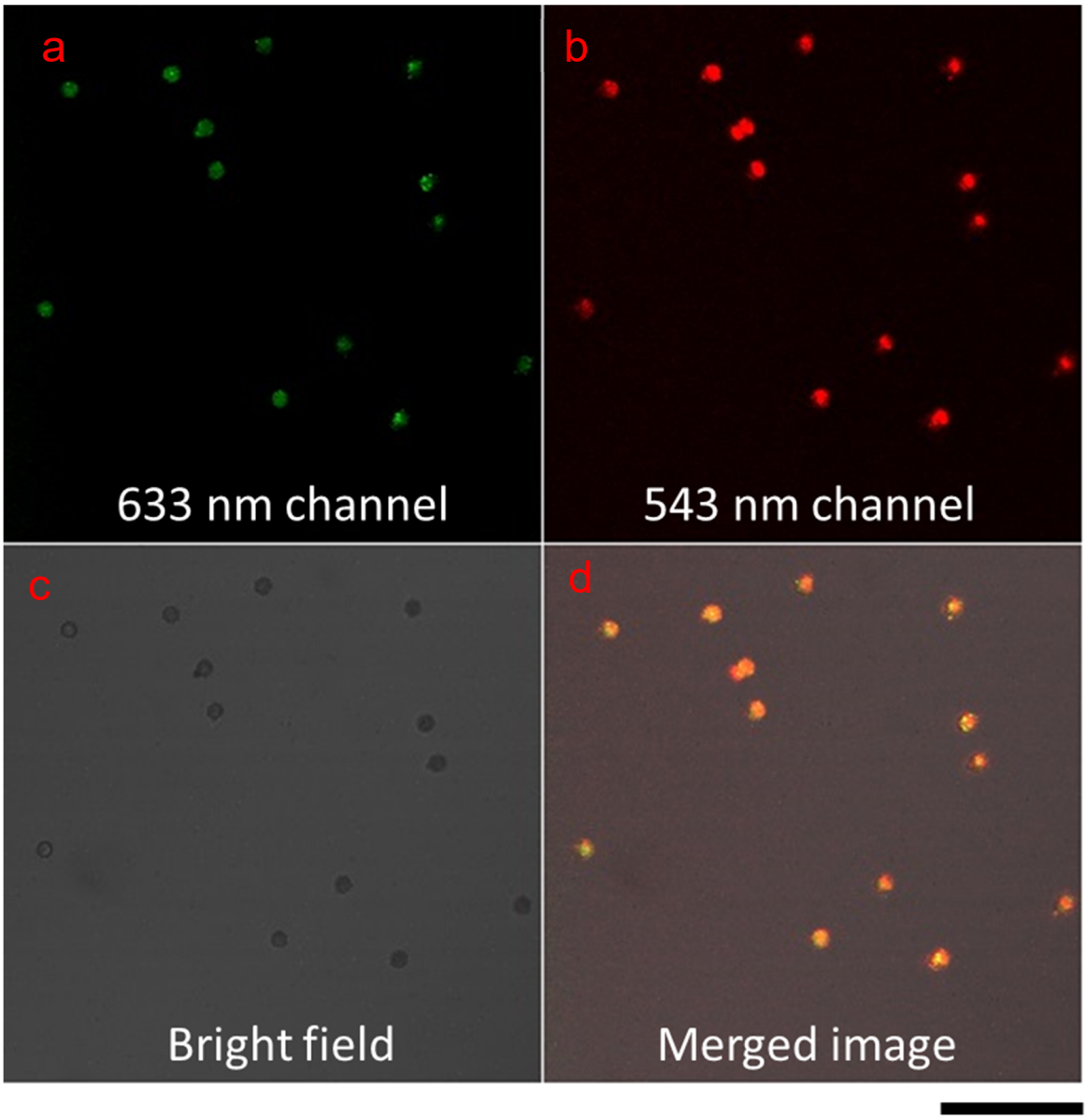

Figure S21. Fluorescence images of the Luminex microbeads after being stained with plasmonic-fluor-Cy3, revealing (a) the barcode of the microbeads (excited by 633 nm laser) of different emission intensities and (b) the fluorescence of bound Cy3 (excited by 543 nm laser). (c) Bright field image of the microbeads. (d) Merged image of bright field and fluorescence. Scale bar, 50 μm.

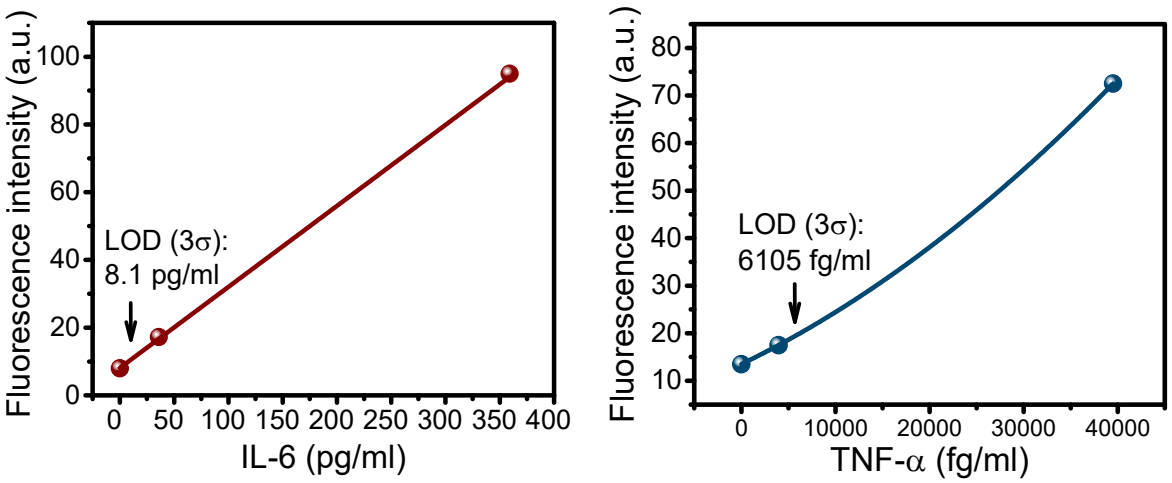

Figure S22. Plot showing the LODs of unenhanced bead-based fluoroimmunoassays (Luminex) for mouse IL-6 and TNF-alpha. The curves were generated using polynomial fitting. Each data point represents the average value of duplicate tests.

Mouse IL-6 Luminex assay				
	Data 1	Data 2	Mean	S.D.
0	8	8	8	0.00
0.359pg/ml	8	9	8.5	0.71
3.59pg/ml	8.5	8	8.25	0.35
35.9pg/ml	16.5	18	17.25	1.06
359pg/ml	96	94	95	1.41

Plasmonic-fluor enhanced mouse IL-6 Luminex assay				
	Data 1	Data 2	Mean	S.D.
0	330	333	331.5	2.12
0.359pg/ml	360	393	376.5	23.33
3.59pg/ml	536	518	527	12.73
35.9pg/ml	815	848	831.5	23.33
359pg/ml	2081	2356	2218.5	194.45

Mouse TNF-α Luminex assay				
	Data 1	Data 2	Mean	S.D.
0	12	15	13.5	2.12
39.5fg/ml	13	14	13.5	0.71
395fg/ml	14	14	14	0.00
3950fg/ml	19	16	17.5	2.12
39500fg/ml	75	70	72.5	3.54

Plasmonic-fluor enhanced mouse TNF-α Luminex assay				
	Data 1	Data 2	Mean	S.D.
0	131	132.5	131.75	1.06
39.5fg/ml	153.5	148.5	151	3.54
395fg/ml	288.5	255.5	272	23.33
3950fg/ml	568	859	713.5	205.77
39500fg/ml	1906	2353	2129.5	316.08

Figure S23. Individual data points, mean value, and standard deviation from mouse IL-6 Luminex, plasmonic-fluor-Cy3 enhanced mouse IL-6 Luminex, mouse TNF-α Luminex, and plasmonic-fluor-Cy3 enhanced mouse TNF-α Luminex assays.

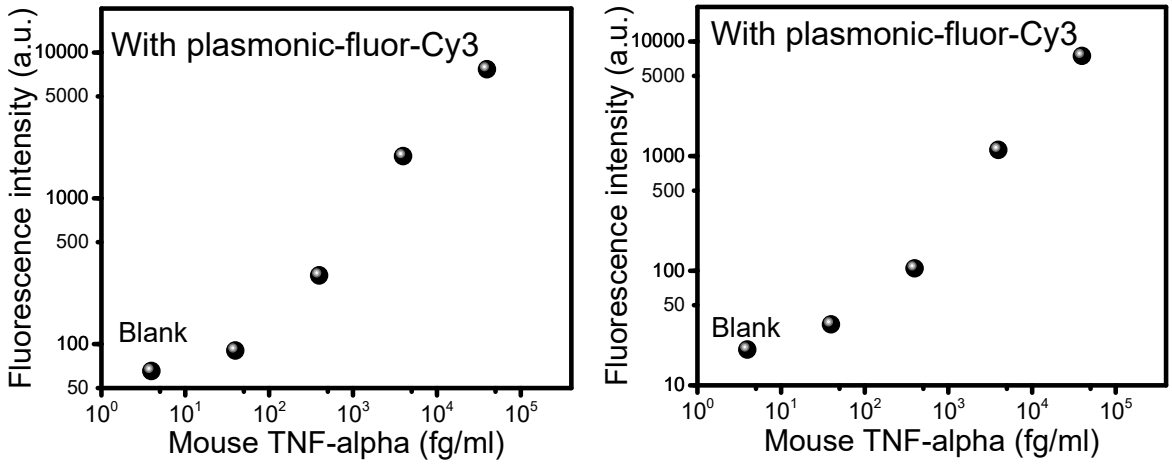

Figure S24. Bead-based mouse TNF-α standard curves obtained after applying plasmonic-fluor-Cy3. The data represents experiments that were performed independently for three times on different days with different batches of plasmonic-fluor-Cy3. Each data point represents the average value of duplicate tests.

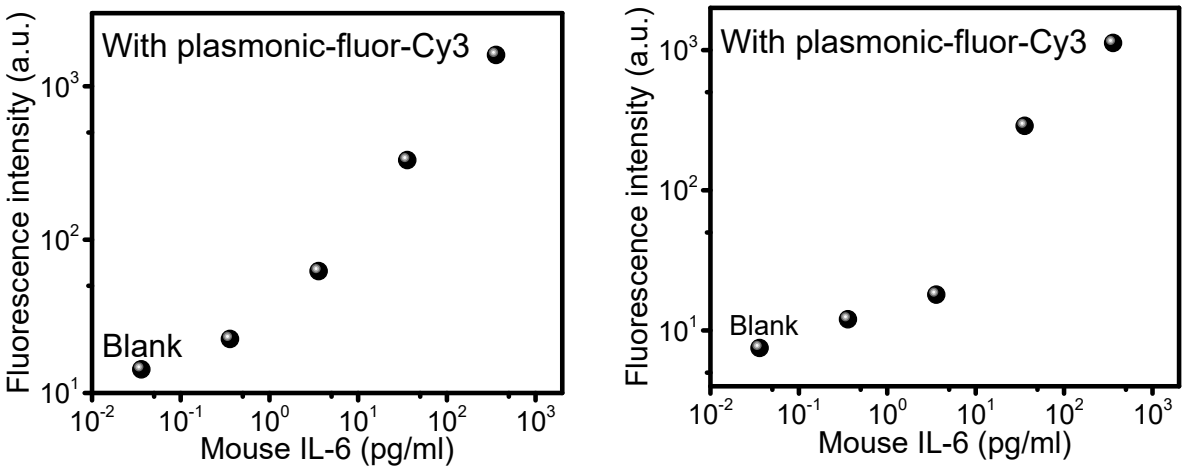

Figure S25. Bead-based mouse IL-6 standard curves obtained after applying plasmonic-fluor-Cy3. The data represents experiments that were performed independently for three times on different days with different batches of plasmonic-fluor-Cy3. Each data point represents the average value of duplicate tests.

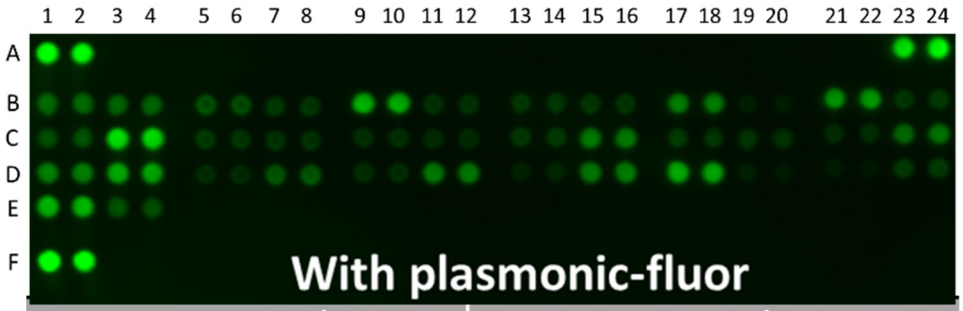

Coordinate	Analyte/Control	Coordinate	Analyte/Control
A1, A2	Reference spots	C15, C16	Lipocalin-2
A23, A24	Reference spots	C17, C18	MCP-1
B1, B2	Adiponectin	C19, C20	MMP-9
B3, B4	ANPEP	C21,C22	Neprilysin
B5, B6	Angiotensinogen	C23, C24	PSA
B7, B8	Annexin V	D1, D2	RAGE
B9, B10	β2-Microglobulin	D3, D4	RBP4
B11, B12	Clusterin	D5, D6	Renin
B13, B14	CXCL16	D7, D8	Resistin
B15, B16	Cyr61	D9, D10	SCF
B17, B18	Cystatin C	D11, D12	Serpin A3
B19, B20	DPPIV	D13, D14	TNF-α
B21, B22	EGF	D15, D16	TNF RI
B23, B24	EGF R	D17, D18	TFF3
C1, C2	FABP1	D19, D20	Thrombospondin-1
C3, C4	Fetuin A	D21, D22	TWEAK
C5, C6	GROa	D23, D24	uPA
C7, C8	IL-1ra	E1, E2	VCAM-1
C9, C10	IL-6	E3, E4	VEGF
C11, C12	IL-10	F1, F2	Reference Spots
C13, C14	TIM-1	F23, F24	PBS (Negative Control)

Figure S26. Identification of specific analytes (or control) of each pair of fluorescence spots on the kidney biomarker array.

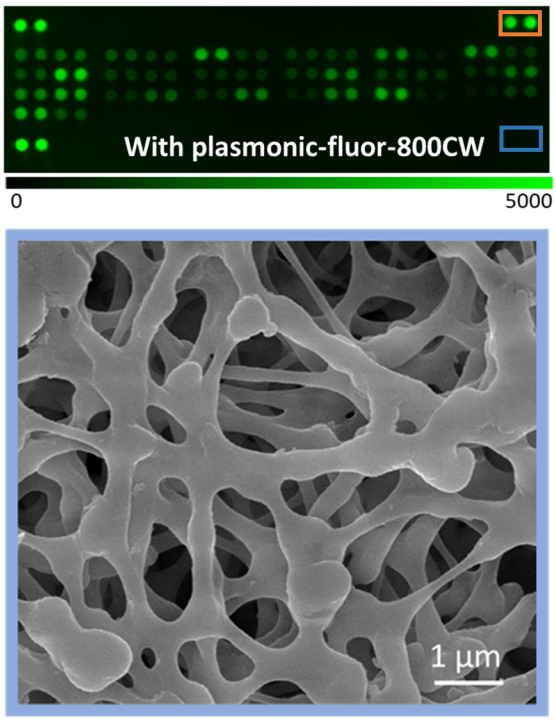

Figure S27. SEM showing the nitrocellulose membrane in the negative control region (blue box; note the absence of fluorescence signal and plasmonic-fluors-800CW) after the addition of plasmonic-fluors-800CW, indicating the low non-specific binding of the plasmonic-fluor-800CW.

	With fluor			
	Data 1	Data 2	Mean	S.D.
Adiponectin	200	30	115	120.21
ANPEP	146	44	95	72.12
Angiotensinogen	134	240	187	74.95
Annexin V	46	-4	21	35.36
β2-Microglobulin	2000	2030	2015	21.21
Clusterin	-28	-30	-29	1.41
CXCL16	-24	-22	-23	1.41
Cyr61	-28	-12	-20	11.31
Cystatin C	268	262	265	4.24
DPPIV	-38	144	53	128.69
EGF	584	602	593	12.73
EGF R	28	52	40	16.97
FABP1	124	168	146	31.11
Fetuin A	1290	1360	1325	49.50
GROα	130	10	70	84.85
IL-1ra	34	-18	8	36.77
IL-6	-20	-26	-23	4.24
IL-10	-24	-32	-28	5.66
TIM-1	16	-2	7	12.73
Lipocalin-2	152	150	151	1.41
MCP-1	-12	-18	-15	4.24
MMP-9	-28	-30	-29	1.41
Neprilysin	-16	-10	-13	4.24
PSA	260	250	255	7.07
RAGE	258	290	274	22.63
RBP4	478	554	516	53.74
Renin	-16	100	42	82.02
Resistin	150	114	132	25.46
SCF	-24	-12	-18	8.49
Serpin A3	316	340	328	16.97
TNF-α	-22	-24	-23	1.41
TNF RI	272	306	289	24.04
TFF3	969	998	983.5	20.51
Thrombospondin-1	-32	-52	-42	14.14
TWEAK	-16	-30	-23	9.90
uPA	42	38	40	2.83
VCAM-1	667	677	672	7.07
VEGF	62	152	107	63.64

	With plasmonic-fluor			
	Data 1	Data 2	Mean	S.D.
Adiponectin	55500	57800	56650	1626.35
ANPEP	55300	54100	54700	848.53
Angiotensinogen	46100	44400	45250	1202.08
Annexin V	29000	28000	28500	707.11
β2-Microglobulin	117000	110000	113500	4949.75
Clusterin	25500	24800	25150	494.97
CXCL16	25300	25200	25250	70.71
Cyr61	27700	26300	27000	989.95
Cystatin C	73900	73200	73550	494.97
DPPIV	10600	9550	10075	742.46
EGF	85700	91200	88450	3889.09
EGF R	25800	26600	26200	565.69
FABP1	35600	38400	37000	1979.90
Fetuin A	141000	136000	138500	3535.53
GROα	29800	27800	28800	1414.21
IL-1ra	26200	26300	26250	70.71
IL-6	24200	24500	24350	212.13
IL-10	22100	21300	21700	565.69
TIM-1	27100	28400	27750	919.24
Lipocalin-2	72700	73300	73000	424.26
MCP-1	28100	24500	26300	2545.58
MMP-9	26500	23600	25050	2050.61
Neprilysin	20500	20700	20600	141.42
PSA	58200	65900	62050	5444.72
RAGE	75800	73700	74750	1484.92
RBP4	105000	106000	105500	707.11
Renin	19600	19800	19700	141.42
Resistin	47400	49700	48550	1626.35
SCF	23300	22500	22900	565.69
Serpin A3	78500	77500	78000	707.11
TNF-α	14000	16100	15050	1484.92
TNF RI	74600	80300	77450	4030.51
TFF3	110000	104000	107000	4242.64
Thrombospondin-1	11400	9070	10235	1647.56
TWEAK	9090	8830	8960	183.85
uPA	30300	31600	30950	919.24
VCAM-1	121000	120000	120500	707.11
VEGF	43700	39600	41650	2899.14

Figure S28: Individual data points, mean value, and standard deviation from Figure 4G (left) and 4H (right).

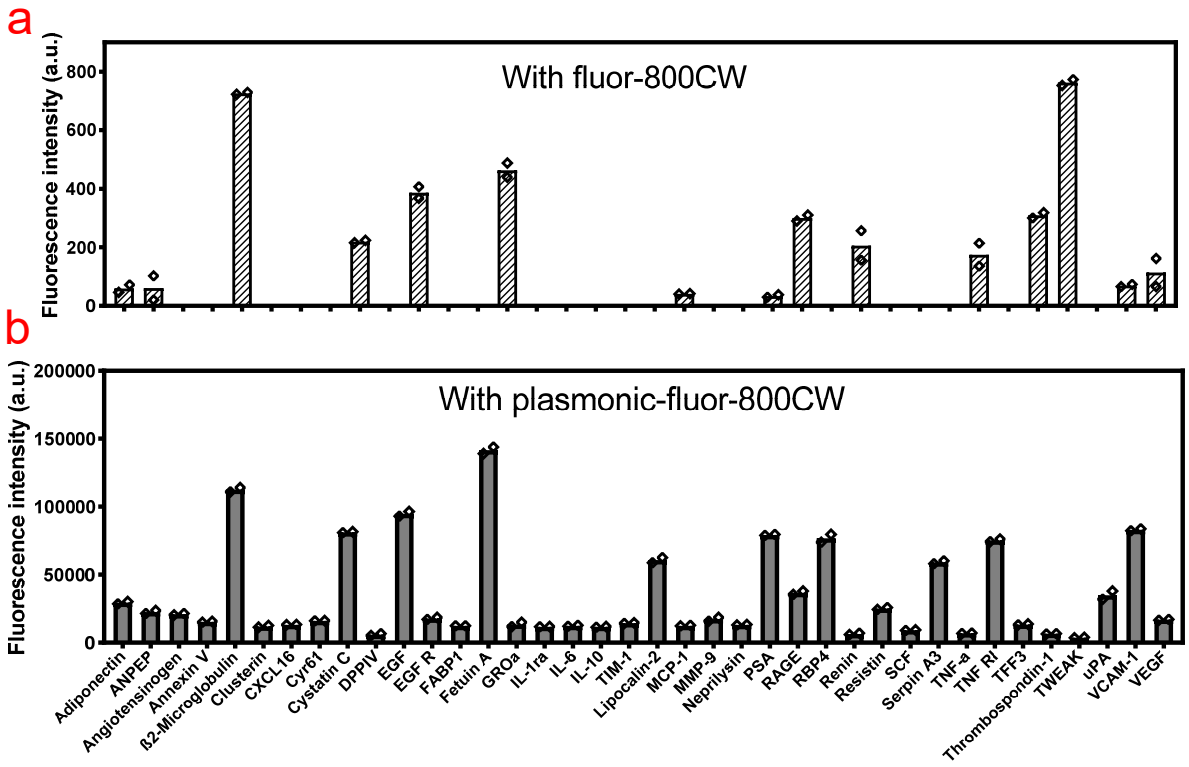

Figure S29. Second independent experiment of kidney biomarker array. Fluorescence intensity corresponding to the concentrations of various urinary biomarkers (A) before (typical assay using conventional fluorophore) and (B) after the addition of plasmonic-fluor-800CW.

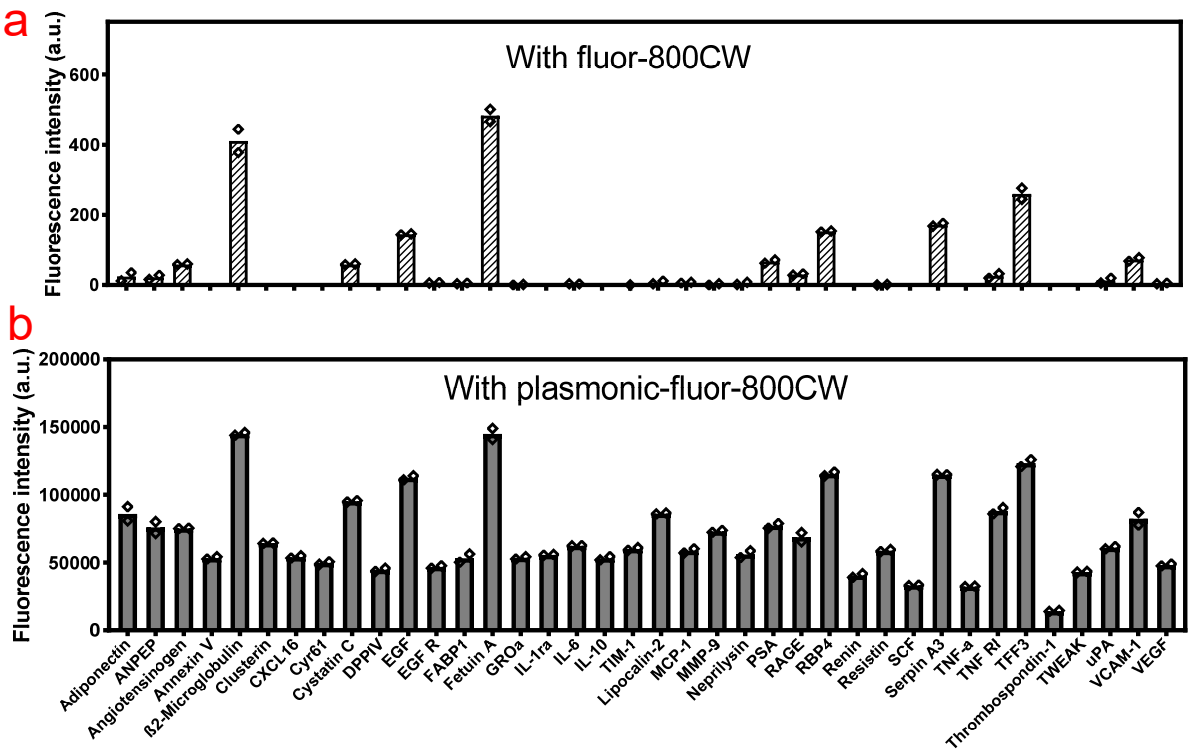

Figure S30. Third independent experiment of kidney biomarker array. Fluorescence intensity corresponding to the concentrations of various urinary biomarkers (A) before (typical assay using conventional fluorophore) and (B) after the addition of plasmonic-fluor-800CW.

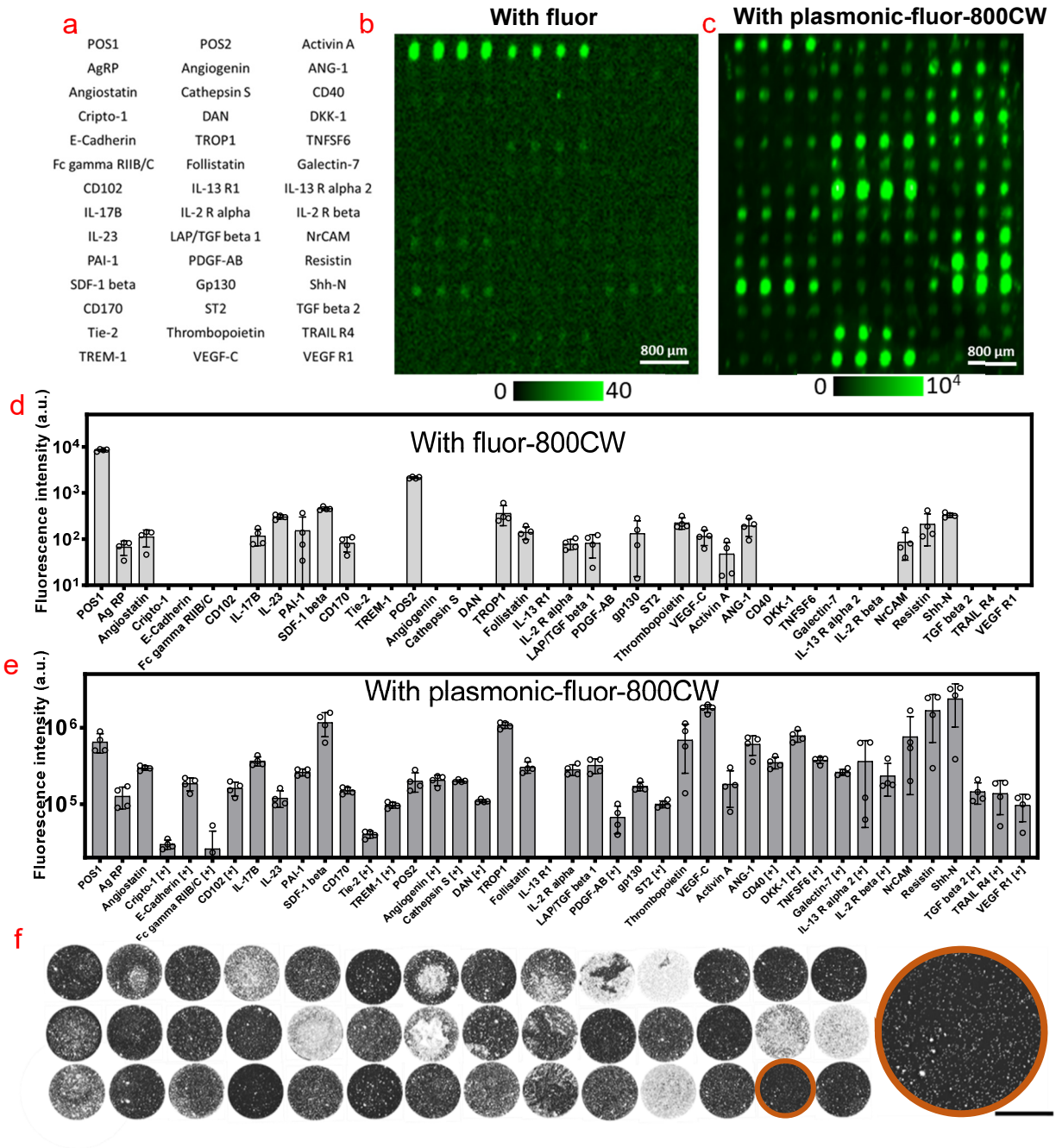

Figure S31. (a) Layout of 40-plex cytokine microarray. Each antibody is printed in quadruplicate horizontally with each spot diameter around 140 μm. Fluorescence map of cytokine microarray obtained (b) using conventional fluorophore (streptavidin-800CW) and (c) after addition of plasmonic-fluor-800CW. Plot showing the fluorescence intensity corresponding to each cytokine obtained (d) using conventional fluorophore (streptavidin-800CW) and (e) after the addition of plasmonic-fluor-800CW. Error bar, s.d. (n=4 repeated tests). (f) Dark field scattering of plasmonic-fluor-800CW (AuNR) absorbed on cytokine microarray. Each circle corresponds to one micro-spot area of each analyte. Scale bar, 50 μm. The distribution of AuNR (plasmonic-fluor-800CW) on each micro-spot can be revealed clearly and counted digitally.

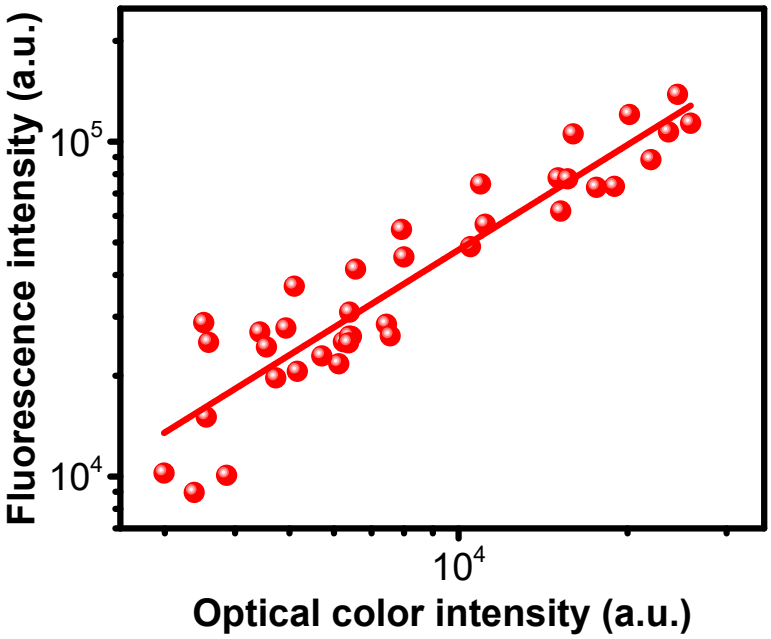

Figure S32. Plot showing the correlation between two readout modes of the kidney biomarker array (fluorescence vs. colorimetric readout).

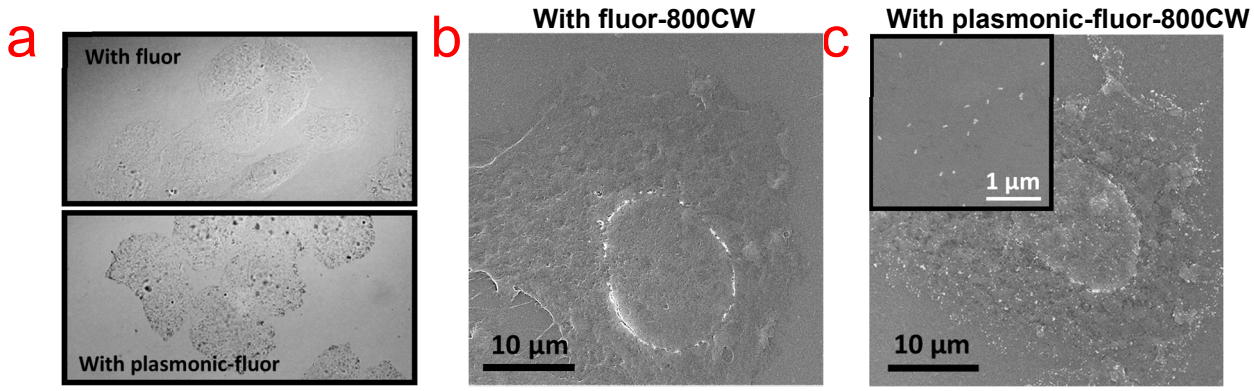

Figure S33. (a) Microscopic bright-field images of SK-BR-3 cells before (top) and after (bottom) being labeled with plasmonic-fluor-800CW. SEM image of (b) conventional fluor labeled SK-BR-3 cell and (c) plasmonic-fluor-800CW labeled SK-BR-3 cell, showing the uniformly distributed plasmonic-fluors on the cell membrane.

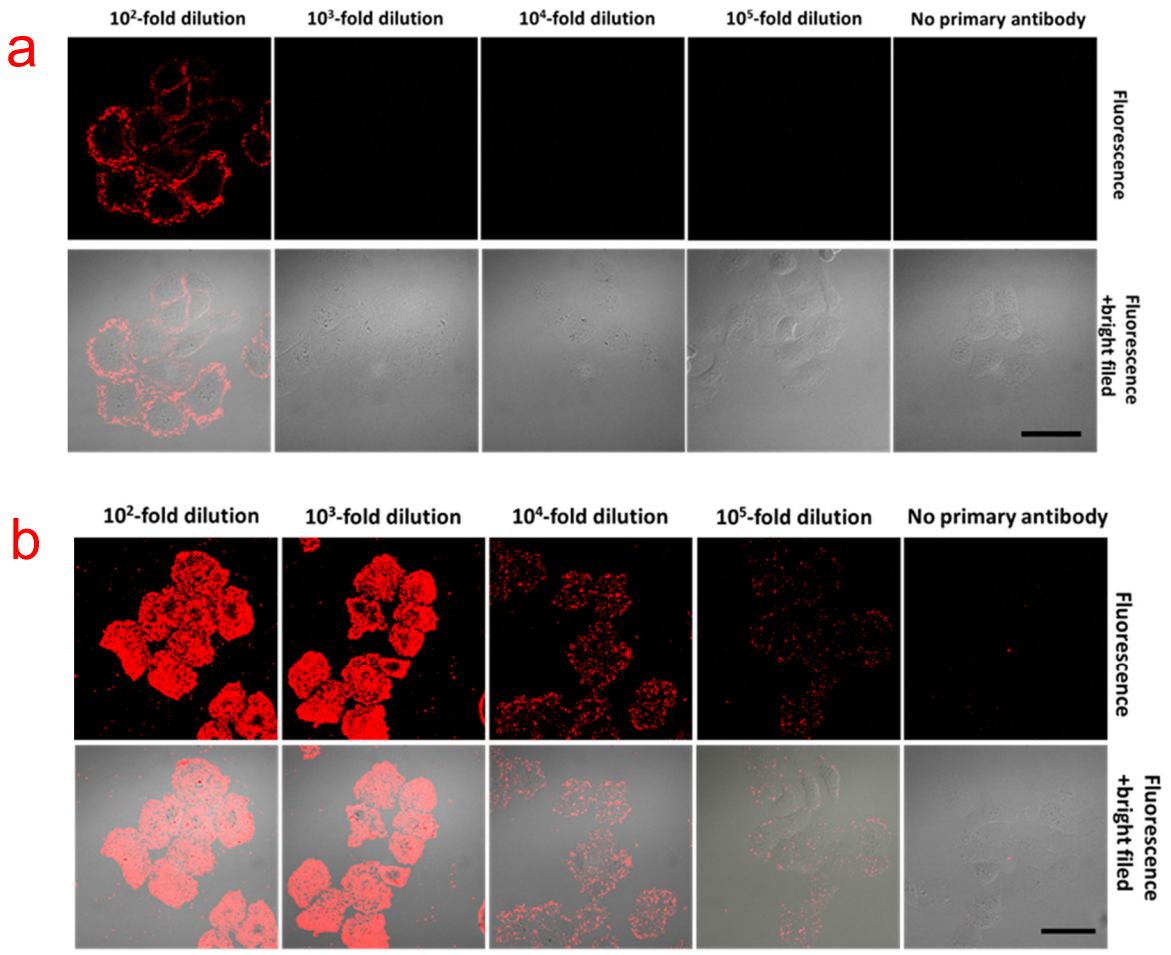

Figure S34. Confocal laser scanning microscopy (CLSM) images of ErbB2 stained breast cancer cells (SK-BR-3) obtained (a) using conventional immunocytochemistry procedure (cells are labelled with biotinylated primary antibody and streptavidin-fluor (800CW) sequentially) (b) followed by the addition of plasmonic-fluor-800CW at different dilutions of ERbB2 primary antibody. Scale bar, 15 μm.

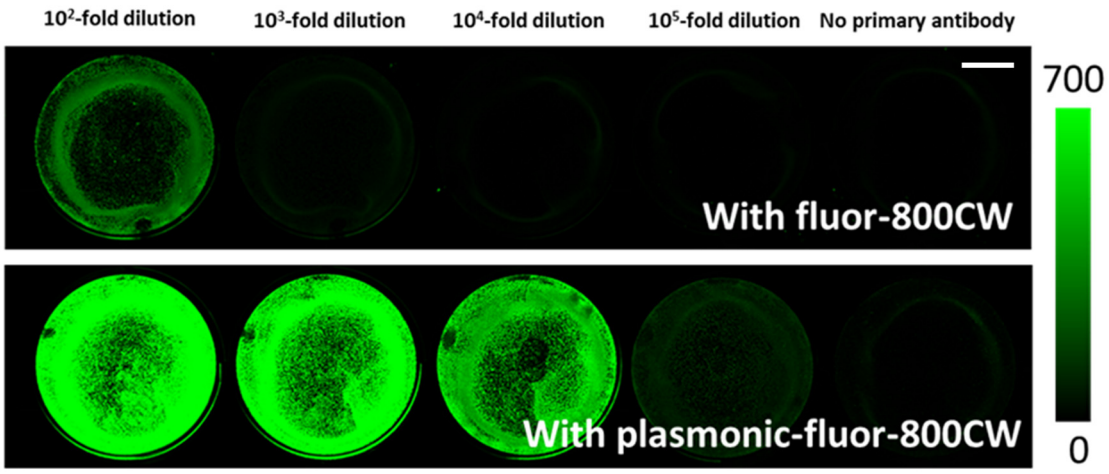

Figure S35. Fluorescence mapping of SK-BR-3 cells cultured on a 6-well plate. The cells are probed with conventional fluorophores (top) followed with plasmonic-fluor-800CW (bottom). Scale bar, 1 cm.

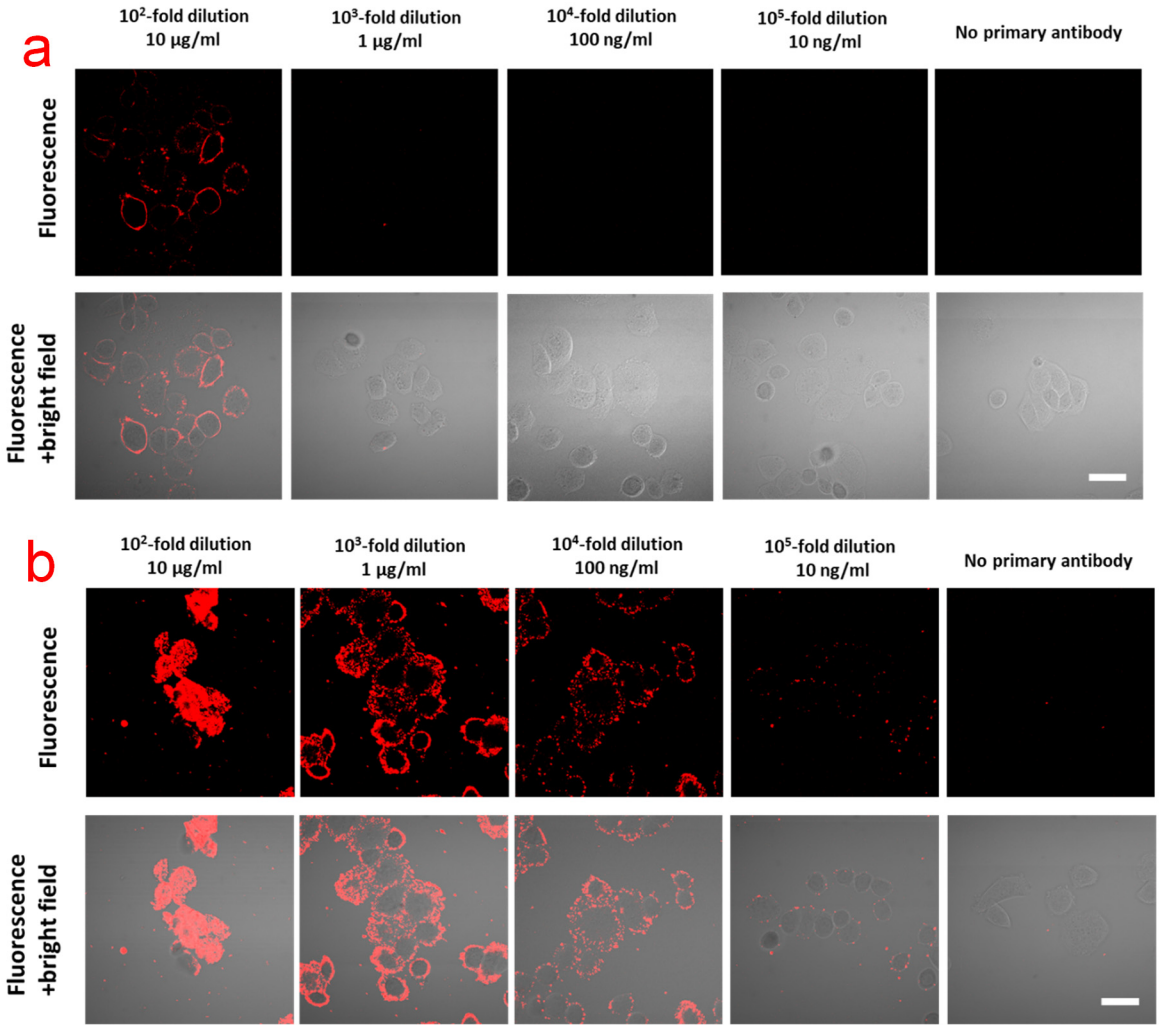

Figure S36. Second independent immunocytochemistry experiment. Confocal laser scanning microscopy (CLSM) images of ErbB2 stained breast cancer cells (SK-BR-3) obtained (a) using conventional immunocytochemistry procedure (cells are labelled with biotinylated primary antibody and streptavidin-fluor (800CW) sequentially) (b) followed by the addition of plasmonic-fluor-800CW at different dilutions of ERbB2 primary antibody. Scale bar, 15 µm.

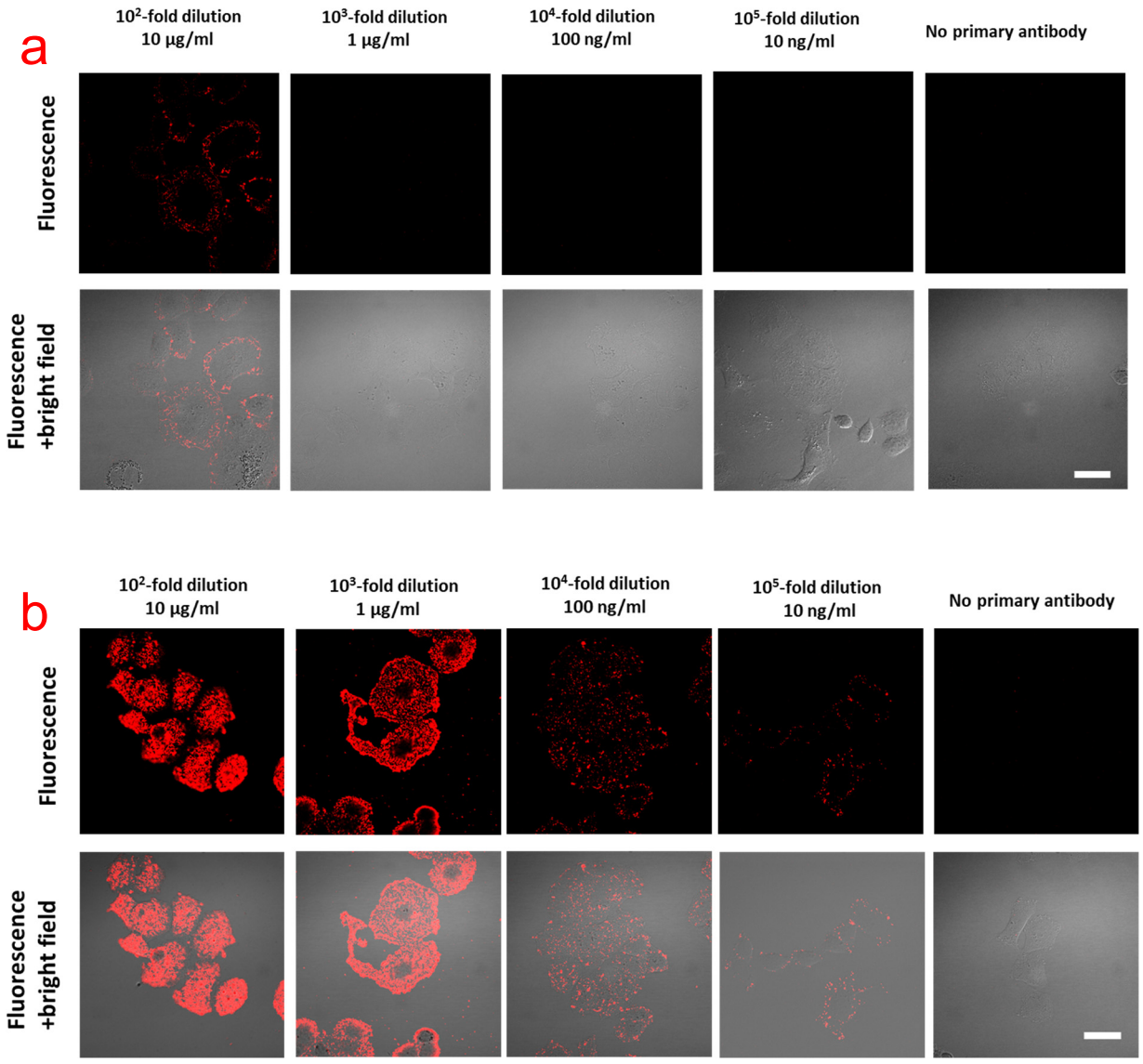

Figure S37. Third independent immunocytochemistry experiment. Confocal laser scanning microscopy (CLSM) images of ErbB2 stained breast cancer cells (SK-BR-3) obtained (a) using conventional immunocytochemistry procedure (cells are labelled with biotinylated primary antibody and streptavidin-fluor (800CW) sequentially) (b) followed by the addition of plasmonic-fluor-800CW at different dilutions of ERbB2 primary antibody. Scale bar, 15 µm.

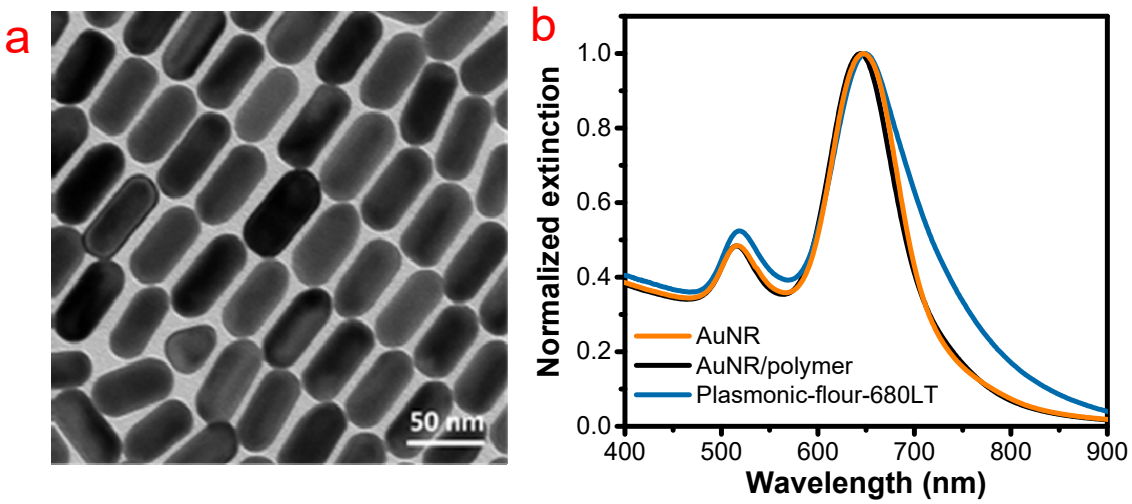

Figure S38. (a) TEM image of AuNR employed for the synthesis of plasmonic-fluor-680LT. (b) UV-vis spectra showing the red shift of AuNR LSPR wavelength after sequential coating of polymer and BSA-biotin-680LT.

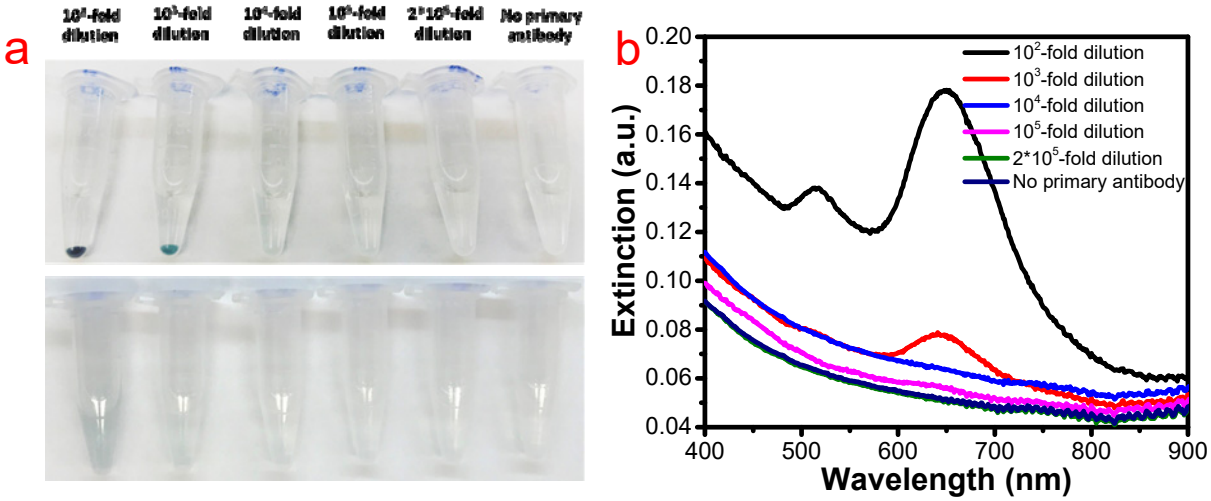

Figure S39. (a) Photographs showing the color change of SK-BR-3 cell (top: pellet; bottom: suspension) after being labeled with plasmonic-fluor-680LT. (b) Vis-NIR extinction spectra of plasmonic-fluor-680LT labeled SK-BR-3 cell suspensions under different dilutions of ErbB2 primary antibody.

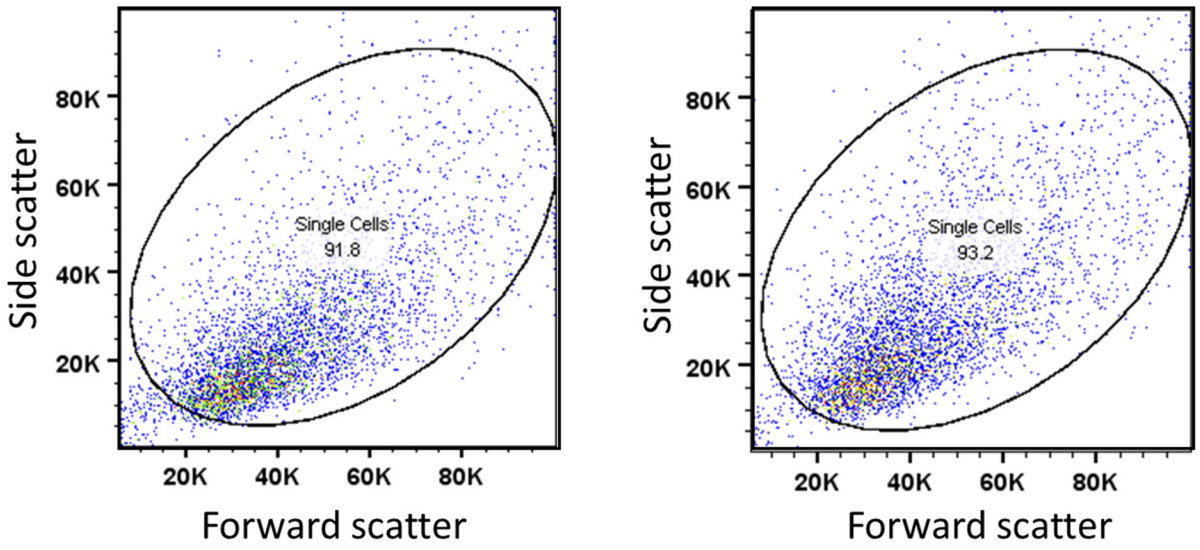

Figure S40. Pseudocolor plots (with example of gating strategy to include single cell) of side scatter and forward scatter of SK-BR-3 cells before (left) and after (right) being labeled with plasmonic-fluor-680LT, showing no obvious change in their size profiles.

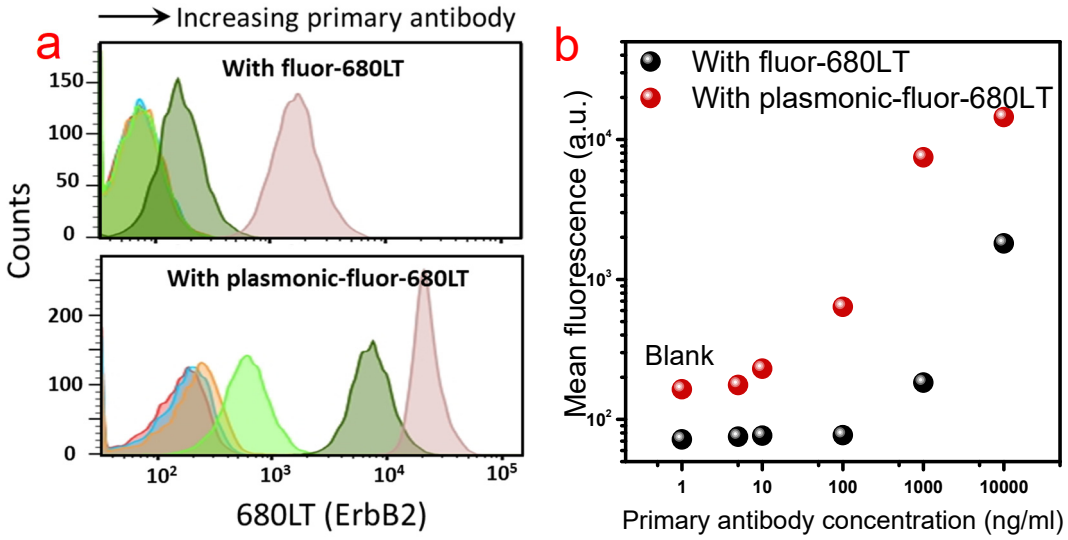

Figure S41. Second independent SK-BR-3 flow cytometry experiment. (a) Histogram showing fluorescence of SK-BR-3 cells before (top) and after (bottom) the addition of plasmonic-fluor-680LT. Red: no primary antibody; blue: 2×10^5-fold dilution; orange: 10^5-fold dilution; light green: 10^4-fold dilution; green: 10^3-fold dilution; rose: 10^2-fold dilution of the stock solution provided by the vendor (1 mg/ml). (b) Plot showing the mean fluorescence intensity obtained from flow cytometry at different primary antibody concentrations.

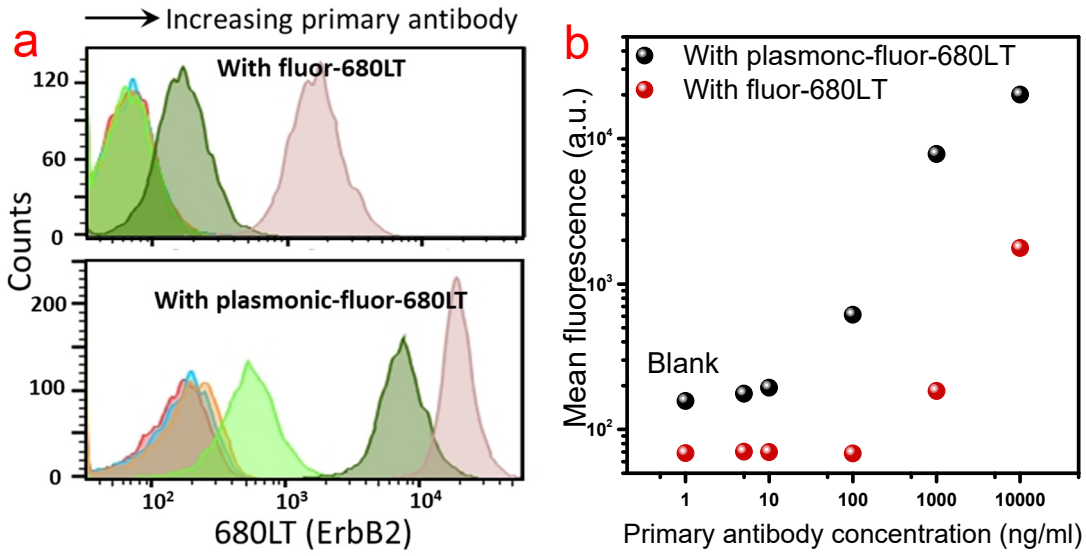

Figure S42. Third independent SK-BR-3 flow cytometry experiment. (a) Histogram showing fluorescence of SK-BR-3 cells before (top) and after (bottom) the addition of plasmonic-fluor-680LT. Red: no primary antibody; blue: 2×10^5-fold dilution; orange: 10^5-fold dilution; light green: 10^4-fold dilution; green: 10^3-fold dilution; rose: 10^2-fold dilution of the stock solution provided by the vendor (1 mg/ml). (b) Plot showing the mean fluorescence intensity obtained from flow cytometry at different primary antibody concentrations.

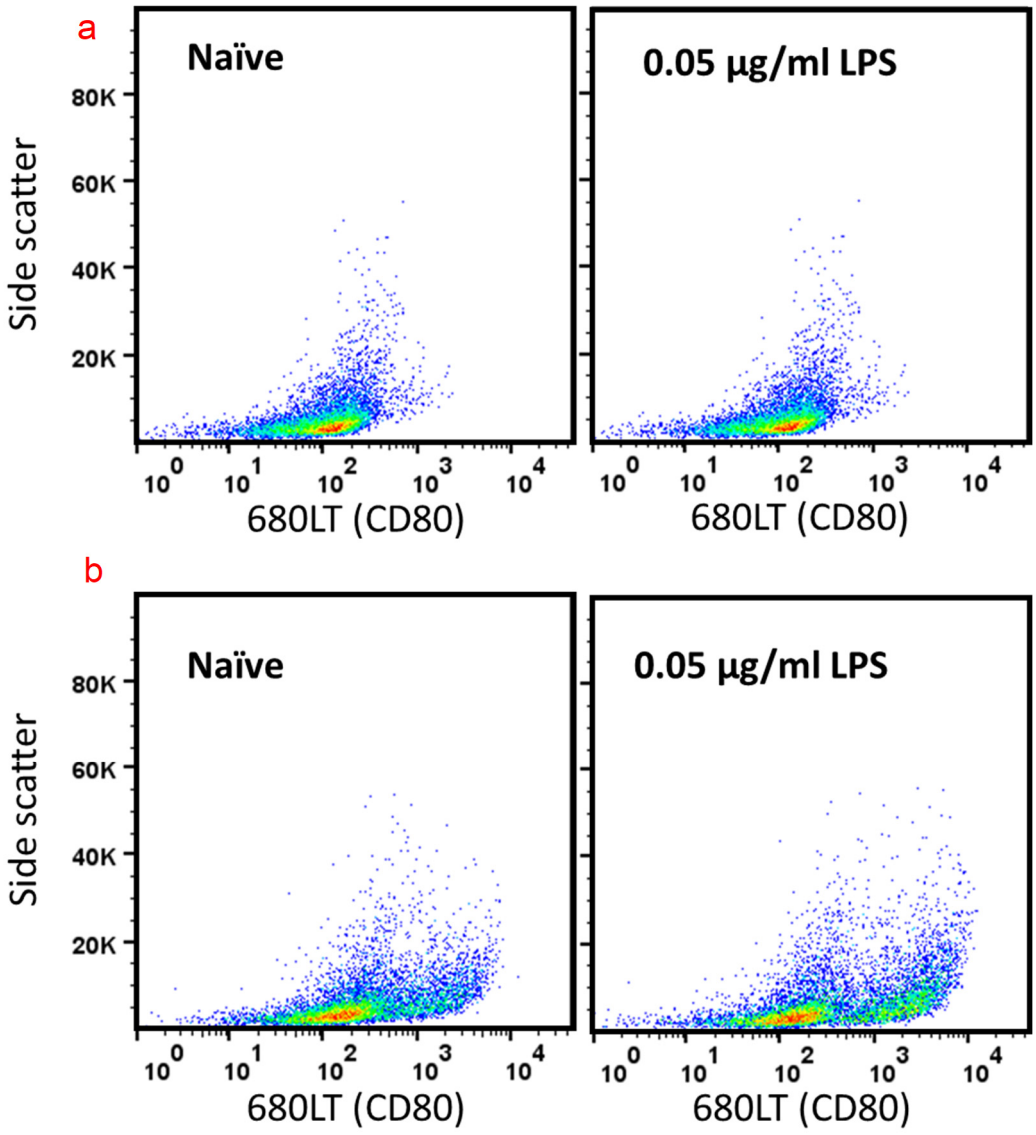

Figure S43. Pseudocolor plots showing the side scatter vs. CD80 fluorescence of BMDC population without LPS stimulation (left: naïve) and after being treated with 0.05 µg/ml LPS (right) using (a) conventional immunofluorescence staining and (b) plasmonic-fluor-680LT.

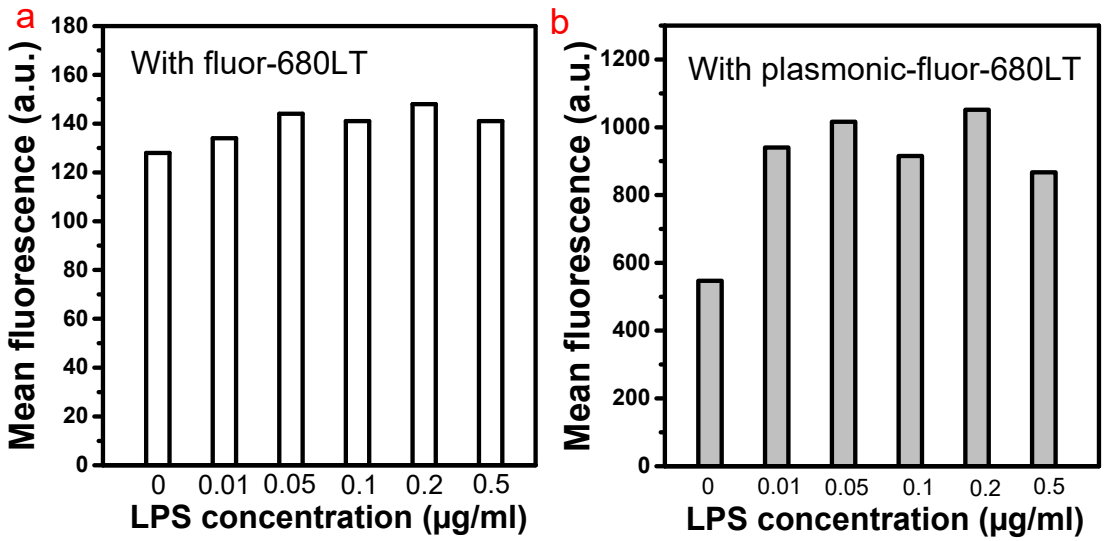

Figure S44. Plot showing mean fluorescence of BMDCs (corresponding to the expression level of CD80) after being stimulated with different amounts of LPS. The BMDCs were probed using (a) conventional immunofluorescence staining and followed by (b) plasmonic-fluor-680LT.

Mouse IL-12 ELISA						
	Abs. 1	Abs. 2	Conc. 1	Conc. 2	Mean	S.D.
Blank	0.47	0.44	5.38	-36.75	0.00	0.00
LPS 0.01 µg/ml	0.63	0.63	207.75	207.13	207.44	0.44
LPS 0.05 µg/ml	0.90	0.94	549.00	599.63	574.31	35.80
LPS 0.1 µg/ml	1.15	1.10	853.88	789.00	821.44	45.87
LPS 0.2 µg/ml	1.28	1.24	1017.25	969.25	993.25	33.94
LPS 0.5 µg/ml	1.26	1.23	994.63	955.00	974.81	28.02

Mouse TNF-α ELISA						
	Abs. 1	Abs. 2	Conc. 1	Conc. 2	Mean	S.D.
Blank	0.07	0.07	-40.50	-27.50	0.00	0.00
LPS 0.01 µg/ml	0.07	0.08	-10.00	-0.50	0.00	0.00
LPS 0.05 µg/ml	0.16	0.15	438.00	360.50	399.25	54.80
LPS 0.1 µg/ml	0.27	0.30	953.00	1119.00	1036.00	117.38
LPS 0.2 µg/ml	0.40	0.39	1624.50	1571.50	1598.00	37.48
LPS 0.5 µg/ml	0.41	0.40	1690.00	1631.50	1660.75	41.37

Figure S45: Individual data points (absorbance and concentration), mean concentration, and standard deviation of ELISA results corresponding to the secreted inflammatory cytokines after LPS stimulation.

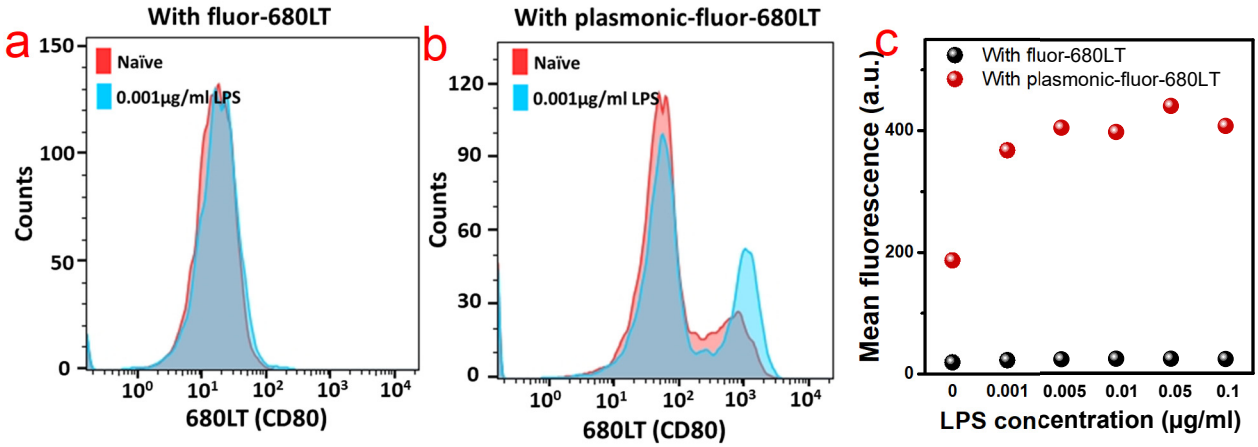

Figure S46. Second independent flow cytometry measurement of BMDC maturation maker probed by plasmonic-fluor-680LT. Fluorescence intensity distribution corresponding to naïve (control) and LPS-stimulated BMDCs obtained using (a) conventional fluors (680LT) and (b) plasmonic-fluor-680LT. (c) Plot showing mean fluorescence intensity of BMDCs (corresponding to the expression level of CD80) after stimulation with different amounts of LPS.

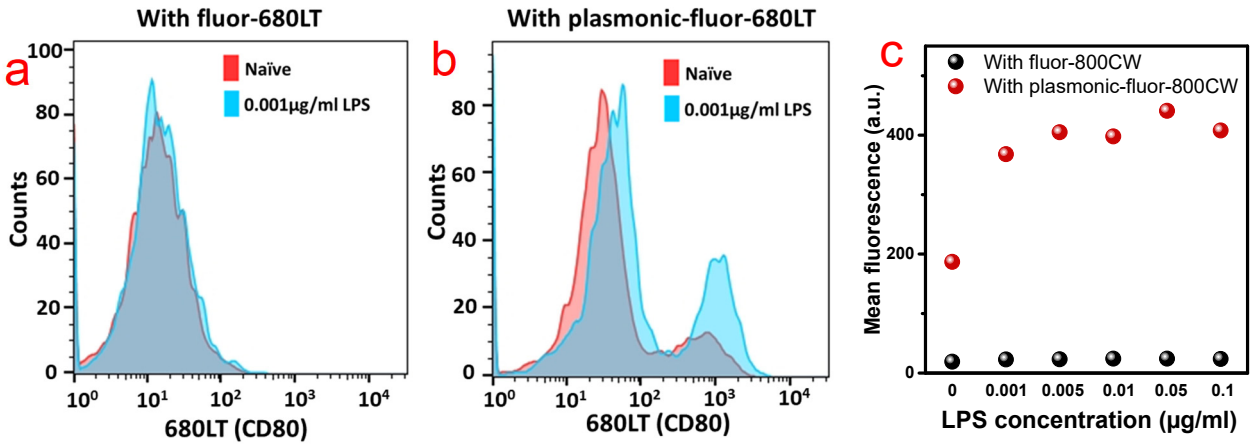

Figure S47. Third independent flow cytometry measurement of BMDC maturation maker probed by plasmonic-fluor-680LT. Fluorescence intensity distribution corresponding to naïve (control) and LPS-stimulated BMDCs obtained using (a) conventional fluors (680LT) and (b) plasmonic-fluor-680LT. (c) Plot showing mean fluorescence intensity of BMDCs (corresponding to the expression level of CD80) after stimulation with different amounts of LPS.

Enhancement factor	Interpretation
30	Fluorescence enhancement factor per 800CW fluorophore (in the form of plasmonic-fluor-800CW)
70	Ratio of fluorescence enhancement factor of AuNR-plasmonic-fluor-800CW to that of AuNP-plasmonic-fluor-800CW
6500	Fluorescence enhancement of a single plasmonic-fluor-800CW compared to single 800CW fluorophore. This value is revised as 6700 (± 900)-fold.
1440	Fluorescence intensity enhancement in human IL-6 p-FLISA compared to conventional FLISA (at IL-6 concentration ~6 ng/ml). This enhancement factor is specific to the IL-6 concentration indicated. At lower concentrations, the enhancement is much higher as described above.
4750	Improvement in the limit-of-detection of human IL-6 using p-FLISA compared to conventional FLISA

Table S2. Interpretation of enhancement factors mentioned in the manuscript.

References

1 Lee, H., Berezin, M. Y., Henary, M., Strekowski, L. & Achilefu, S. Fluorescence lifetime properties of near-infrared cyanine dyes in relation to their structures. *Journal of Photochemistry and Photobiology A: Chemistry* **200**, 438-444 (2008).

2 Tang, R., Lee, H. & Achilefu, S. Induction of pH sensitivity on the fluorescence lifetime of quantum dots by NIR fluorescent dyes. *Journal of the American Chemical Society* **134**, 4545-4548 (2012).

3 Bardhan, R., Grady, N. K., Cole, J. R., Joshi, A. & Halas, N. J. Fluorescence enhancement by Au nanostructures: nanoshells and nanorods. *ACS nano* **3**, 744-752 (2009).

4 Near, R. D., Hayden, S. C., Hunter Jr, R. E., Thackston, D. & El-Sayed, M. A. Rapid and efficient prediction of optical extinction coefficients for gold nanospheres and gold nanorods. *The Journal of Physical Chemistry C* **117**, 23950-23955 (2013).

5 Park, K., Biswas, S., Kanel, S., Nepal, D. & Vaia, R. A. Engineering the optical properties of gold nanorods: independent tuning of surface plasmon energy, extinction coefficient, and scattering cross section. *The Journal of Physical Chemistry C* **118**, 5918-5926 (2014).

6 Orendorff, C. J. & Murphy, C. J. Quantitation of metal content in the silver-assisted growth of gold nanorods. *The Journal of Physical Chemistry B* **110**, 3990-3994 (2006).